

Optimal work extraction in measurement-based quantum Otto engines: Non-adiabaticity and generalized measurements can be beneficial

Arunabha Das^{1,2} , Sayan Mondal^{1,2} ,* Debarupa Saha^{1,2} ,* and Ujjwal Sen^{1,2} 

¹Harish-Chandra Research Institute, Chhatnag Road, Jhansi, Prayagraj 211 019, India

²Homi Bhabha National Institute, Training School Complex, Anushakti Nagar, Mumbai 400 094, India

Measurement-based quantum heat engines have attracted significant interest as alternatives to conventional thermal engines, as they replace the hot thermal reservoir with quantum measurements, thereby offering greater controllability and simpler implementation. Motivated by these advantages, we investigate a measurement-driven quantum Otto engine with a qubit working substance and study the optimal work extractable from such engines, including whether their performance can surpass that of conventional quantum Otto cycles. We analyze the engine in both the infinite-time (adiabatic) and finite-time (non-adiabatic) regimes, considering two distinct implementations obtained through optimization over all projection-valued measurements (PVMs) and over all two-outcome positive operator-valued measurements (POVMs). We show that measurement-based engines can outperform conventional quantum Otto engines within specific parameter regimes and that POVM-based engines can yield higher optimal work extraction than PVM-based ones. Furthermore, by incorporating the thermodynamic cost associated with resetting the auxiliary system required for POVM implementation, we demonstrate that the resulting net work output can still exceed that of PVM-based engines under suitable conditions on the spectral gaps and cold bath temperature. We also identify regimes in which non-adiabatic implementations can yield higher work output and efficiency than their adiabatic counterparts. Our study provides operational guidelines for designing improved measurement-driven quantum Otto engines.

I. INTRODUCTION

Quantum thermodynamics has attracted significant attention due to both its foundational importance [1–4] and its prospect for developing nanoscale technologies for energy storage, transport, and conversion. In this context, a variety of quantum thermal devices have been proposed and extensively investigated, including quantum heat engines [5–16], quantum refrigerators [16–20], quantum transistors [21–26], quantum heat transformers [27, 28], and quantum batteries [29–31]. Among these, quantum heat engines occupy a central role as they provide a fundamental framework for understanding how thermodynamic tasks such as the conversion of heat into useful work can be realized and potentially enhanced in the quantum regime.

The quantum analogs of standard thermodynamic cycles, such as the Carnot [16, 32–35] and Otto [16, 34, 36–43] cycles, have therefore been widely investigated. In this work, we focus on the quantum Otto cycle. In a conventional quantum Otto engine, the working medium undergoes two unitary work strokes interleaved with thermalization strokes involving hot and cold thermal reservoirs. The work strokes are typically assumed to be adiabatic in order to suppress unwanted transitions between instantaneous energy eigenstates. However, truly adiabatic evolution requires long operation times, resulting in vanishingly small output power. Motivated by the need to realize thermal machines operating at finite power, considerable effort has therefore been devoted to the study of finite-time quantum Otto engines and the role of non-adiabatic effects [44–59].

These theoretical developments have been accompanied by rapid experimental progress. Quantum Otto engines and re-

lated thermal cycles have been experimentally implemented using superconducting quantum circuits [60, 61], ultracold atomic systems [62], spin-based platforms [63], optical simulators [64], cavity-QED setups [65], and several other experimentally accessible architectures [66–68]. Such developments have established quantum thermal machines as experimentally relevant systems rather than merely theoretical constructs.

An interesting alternative to conventional quantum Otto engines arises when one of the thermalization strokes, typically the hot-bath stroke, is replaced by a quantum measurement process [69–78]. In such measurement-based quantum Otto engines, energy is injected into the working medium through quantum measurements rather than via thermal contact with a hot reservoir, enabling measurement-induced work extraction under generalized thermodynamic settings. These engines have attracted considerable attention in recent years because quantum measurements offer enhanced controllability, simpler implementation, and the possibility of improved thermodynamic performance. For instance, enhanced output power has been reported in many-body spin-based engines where the thermalization stroke is replaced by a quantum measurement process [78]. Measurement-driven engines have been extensively investigated both in the adiabatic regime [70] and in finite-time non-adiabatic settings [74–76].

The measurements employed in such engines can be either projective-valued (PV) measurements [71–76] or more general positive operator-valued measurements (POVMs) [77–79]. Existing studies have demonstrated that measurement-based engines can outperform conventional hot-bath-driven Otto engines in terms of extractable work and efficiency. However, most previous studies focus on specific measurement protocols or restricted parameter regimes, and a systematic characterization of optimal work extraction in measurement-driven engines remains largely unexplored, particularly in finite-time non-adiabatic regimes. This natu-

* These authors contributed equally to this work.

rally raises several fundamental questions: What is the maximum work extractable from measurement-based quantum Otto engines? How does this optimum compare across PVM-, POVM-, and conventional two-bath Otto engines? Furthermore, how is the performance modified once the thermodynamic cost associated with implementing measurements is taken into account?

Motivated by these open questions, in the present work we investigate measurement-based quantum Otto engines in which the hot-bath thermalization stroke is replaced by a quantum measurement process. Considering a single-qubit working substance, we analyze both projective-valued measurements (PVMs) and generalized two-outcome POVMs based quantum Otto engines, and derive the corresponding conditions for optimal work extraction in both the adiabatic and non-adiabatic regimes.

We first show that, in the adiabatic limit, the efficiency of measurement-based Otto engines remains identical to that of conventional two-bath Otto engines. We then examine whether such engines can nevertheless provide enhanced work extraction. In this regard, we also investigate finite-time measurement-based Otto cycles, where the unitary work strokes are intrinsically non-adiabatic, and compare with their conventional two-bath counterparts. In particular, we demonstrate that the maximum work obtainable using PV measurements always exceeds that of conventional Otto engines operating with finite-temperature hot baths, in the adiabatic limit as well as in the non-adiabatic regimes.

Moreover, we demonstrate that POVM-based Otto engines can yield even higher optimal work than PVM-based ones, not only in the adiabatic limit but also in non-adiabatic regimes. Particularly, we identify that, in the adiabatic limit, POVM-based Otto engines can yield even higher optimal work than their PVM-based counterparts under suitable conditions based on the cold bath temperature and the spectral gaps of the setup, even when the thermodynamic cost to recycle the auxiliary system required for the POVM-implementation is considered.

Furthermore, in case of measurement-based engines, non-adiabatic implementations can yield higher work output and efficiency than their adiabatic counterparts, and in particular, we identify the corresponding conditions in case of PVM-fueled Otto engines. Also, measurement-fueled Otto cycles can operate as engines even in parameter regimes where conventional Otto cycles fail to operate as engines. Finally, we provide a detailed comparative analysis of conventional two-bath, PVM-based, and POVM-based Otto engines in both adiabatic and non-adiabatic regimes, thereby identifying the operational regimes where measurement-driven quantum thermal machines exhibit enhanced thermodynamic performance.

The remainder of the paper is organized as follows. In Sec. II, we introduce the necessary preliminaries, including the framework of quantum measurements and the traditional Otto cycle. In Sec. III, we demonstrate that the efficiency of measurement-based Otto engines in the adiabatic regime remains identical to that of the traditional two-bath Otto engine. The optimization of work extraction for PV- and POVM-based engines is presented in Secs. IV and V, respectively. A comparative analysis of the three types of engines is provided in

Sec. VI. Finally, we conclude in Sec. VII.

II. PRELIMINARIES

In this section, we discuss the notion of PVM and POVM in the context of measurement-based otto engine. We discuss various aspects of the engine including its work output and efficiency.

A. Quantum measurements

In quantum mechanics, any observable O is a hermitian linear operator, that can be spectral-decomposed as $O := \sum_i a_i P_i$, where a_i are the eigenvalues and P_i are the corresponding eigenvectors. It is well known that the eigenvalues of a hermitian operators are real and the corresponding eigenstates are orthonormal and complete. The building block of the PV measurement are these projection operators P_i , which are (i) real $P_i^\dagger = P_i$, (ii) positive $P_i \succ 0$, (iii) complete $\sum_i P_i = I$ and (iv) orthonormal $P_i P_j = \delta_{ij} P_i$. For an arbitrary state ρ , the probability for clicking a particular outcome P_i is given by $p_i = \text{Tr}(P_i \rho)$. This yields the corresponding post-measurement state as $\rho'_i = P_i \rho P_i / p_i$. If the post-measurement outcome is discarded, then the measurement process generates an ensemble given by post-measurement state $\rho_{\text{PM}} := \sum_i p_i \rho'_i = \sum_i P_i \rho P_i$.

The PV measurements do not constitute the most general kind of measurements allowed in quantum mechanics. There exists a more general class of measurements, called POVM in the framework of quantum mechanics. It is characterized by a collection of operators E_i corresponding to the i -th outcome of the measurement. The probability of clicking the i -th outcome is given by $\tilde{p}_i = \text{Tr}(E_i \rho)$. Being more general than PV measurements, POVMs satisfy certain properties as well, such as, (i) positivity $E_i \succeq 0$ and (ii) completeness $\sum_i E_i = I$. The post-measurement state corresponding to the i -th outcome, is given by $\tilde{\rho}_i = M_i \rho M_i / \tilde{p}_i$, where M_i are the Kraus operators, defined as $M_i = \sqrt{E_i}$. The post measurement state without the selection of any particular outcome is given by $\tilde{\rho}' = \sum_i \tilde{p}_i \tilde{\rho}_i = \sum_i M_i \rho M_i^\dagger$. Unlike P_i -s, E_i -s are not necessarily orthogonal to each other. According to Naimark's dilation theorem, any POVM acting on a Hilbert space can be realized as a PV measurement on a larger Hilbert space. It can be performed by coupling with a auxiliary system, then applying a global unitary transformation, and finally doing a PV measurement on the extended Hilbert space associated with the composite system.

B. Otto engines

1. Traditional two bath Otto engines

The conventional Otto cycle consists of four strokes. These involve two heat stroke and two work stroke. In order to extract work the Otto cycle operates with the help of two thermal

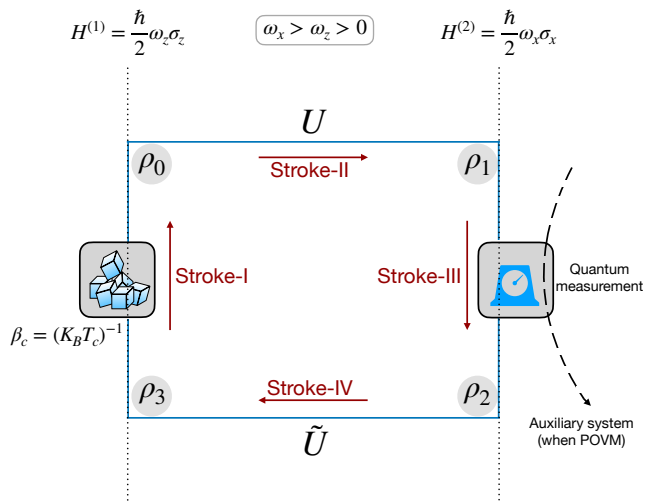


Figure 1. **Schematic diagram of the measurement-based quantum Otto engine.** The measurement-based quantum Otto engine consists of four strokes. In Stroke-I, the working medium thermalizes with a cold bath at temperature T_c . Stroke-II and Stroke-IV are unitary driving strokes, generated through adiabatic or non-adiabatic driving of the Hamiltonian. Since these strokes are entropy conserving, they correspond to the work strokes of the cycle. Stroke-III is the measurement stroke, which replaces the hot-bath thermalization process present in the conventional Otto engine, where the system would otherwise interact with a bath at temperature $T_h > T_c$. The measurement can be either PVM or generalized POVM. In the POVM-based engine, the generalized measurement is implemented using an auxiliary system, represented by the black dotted arrow during Stroke-III. During both Stroke-I and Stroke-III, the Hamiltonian remains fixed, making them isochoric heat strokes.

baths: a hot bath at temperature T_h and a cold bath at temperature T_c , with $T_h > T_c$. The work is extracted by driving the system between two Hamiltonian $H^{(1)}$ and $H^{(2)}$ with varying spectral gap. We briefly discuss the four strokes in the following.

- **Stroke-I.** This is a thermalizing stroke where the system (engine) is put in contact with the cold bath and the Hamiltonian is kept fixed at $H^{(1)}$. In this stroke only heat is exchanged between the engine and the bath.
- **Stroke-II.** After the stroke-I, the engine is isolated from the cold bath. The system Hamiltonian is driven from $H^{(1)}$ to $H^{(2)}$. This leads to a unitary evolution of the system. This is a work stroke.
- **Stroke-III.** This is a thermalizing stroke, where the system is put in contact with the hot bath. The Hamiltonian is fixed at $H^{(2)}$. Only heat is exchanged between the bath and the system.
- **Stroke-IV.** The system is isolated from the hot bath and the Hamiltonian is driven from $H^{(2)}$ to $H^{(1)}$, thus unitarily evolving the system. This is again a work stroke.

Since the strokes-II and IV are unitary, the entropy of the system do not change. Thus, the change of energies during these

two strokes are considered as work. The total work corresponding to the cycle is the sum total of the work from both of these strokes. The strokes-I and III are thermalizing strokes. Hence, the entropy changes, consequently the change in energy of the system in these strokes contribute to heat. The Otto engine is usually analyzed in the adiabatic regime, i.e., the time taken by each stroke is taken to be very large, hence the evolution of the states in the unitary strokes follow the adiabatic theorem, while the thermalizing strokes completely thermalize the system to the corresponding Gibbs state. Recently, engines involving finite-time strokes have also been studied [55]. In this work, we call such engines to be operating in the non-adiabatic regime. For completeness, we present the detailed analysis of the conventional Otto cycle with two baths in the adiabatic limit in Appendix A, while the analysis including the non-adiabatic regime is given in Appendix B.

2. Measurement-based Otto engines

In a measurement-based Otto cycle, one of the thermalization strokes is replaced by a quantum measurement stroke. The energy exchanged during this process is interpreted as heat, since the measurement changes the entropy of the working medium while the Hamiltonian remains fixed. Depending on the protocol, either the hot bath [69–77, 80] or the cold bath [78] can be replaced by a measurement process. However, both thermalization strokes cannot simultaneously be replaced by measurements. This is because a bare quantum measurement is intrinsically entropy-increasing and, by itself, cannot sustain cyclic engine operation, as established by the no-go theorem [81]. Consequently, an additional entropy-reducing mechanism, such as feedback control or bath-assisted thermalization, is necessary for the engine to operate.

In the current work, the stroke-III of the Otto cycle, i.e., the thermalizing stroke, which involves the hot bath, is replaced with a measurement process. The first two strokes are the same as the conventional Otto cycle. The exchanged energy is incorporated as heat, according to the entropic definition in the context of quantum thermodynamics. Fig. 1 depicts this type of Otto cycle. Besides the projection-valued (PV) measurements, stroke-III can also incorporate projective operator valued measurement (POVM), which can be modeled with the assistance of an auxiliary system. The goal of our work is to find the optimal extractable work from these three classes of engines and provide a comparative study between them.

C. Conventions and notations

Conventions used for work and efficiency. In this work, we adopt the following sign convention. The sum of the works (w_{II} and w_{IV}) associated with the two unitary strokes (II and IV) defines the total work performed during the cycle. Under the standard thermodynamic convention, this quantity is negative when the engine delivers work. To make the engine operation explicit, we redefine the total work as

$w_{\text{total}} = -(w_{\text{II}} + w_{\text{IV}})$, such that a positive value of w_{total} corresponds to net work extraction by the Otto cycle. This convention allows us to directly focus on maximizing the work output. Conversely, when $w_{\text{total}} \leq 0$, the cycle ceases to operate as an engine. Accordingly, the efficiency of the engine is defined as $\eta = w_{\text{total}}/q_h$, where q_h is the heat exchanged in stroke-III.

Notations. Here, we introduce the notations used in the remaining part of the paper. In the adiabatic Otto cycle, we denote the states of the working substance after each stroke by ρ_i^x and their corresponding energies by E_i^x , with $i \in \{0, 1, 2, 3\}$ (see Fig. 1), where $x \in \{\mathcal{C}, \text{II}, \mathcal{P}\}$ represents the type of the Otto cycle. Here, \mathcal{C} , II , and \mathcal{P} corresponds to the conventional (traditional), PVM-based, and POVM-based Otto cycles, respectively. The work associated with strokes-II and IV are denoted by W_1^x and W_2^x , respectively, while the heat exchanged during strokes-I and III are denoted by Q_c^x and Q_h^x , respectively. W^x and η^x denote the total work and the efficiency of the engine, respectively. When we discuss about the non-adiabatic Otto cycle, ρ_i^x , E_i^x , W_1^x , W_2^x , W^x , and η^x are replaced by $\tilde{\rho}_i^x$, \mathcal{E}_i^x , \mathcal{W}_1^x , \mathcal{W}_2^x , \mathcal{W}^x , and η_{na}^x , respectively.

Maximization of any quantity Z over any particular set Y gives the maximum value denoted by Z_M . Similarly, the minimization of any quantity Z over any particular set Y gives the minimum value denoted by Z_m .

Units used in plots. The frequencies considered in this paper are scaled by a characteristic frequency Ω_0 (having dimensions of frequency), such that all frequencies are effectively dimensionless. Consequently, all energies, work, and heat are expressed in the units of $\hbar\Omega_0$ and the temperatures are expressed in the units of $\hbar\Omega_0/k_B$.

III. EFFICIENCY CAN NOT BE ENHANCED IN THE ADIABATIC QUANTUM OTTO CYCLE

In this section, we develop a general framework to analyze the efficiency of the quantum Otto cycle. We consider a quantum Otto engine in which stroke-III may correspond either to a thermalization (to a hot bath) process or to a measurement operation. We show that, irrespective of this distinction, the efficiency remains identical in both cases provided the work strokes are adiabatic.

In order to calculate the efficiency, we need to first find the work output and heat absorbed by the engine. We find that the net output work, $W^x = (1 - \omega_z/\omega_x)(E_2^x - E_1^x)$ is independent of whether the engine operates via a traditional thermal stroke or a measurement-based process.

As discussed previously, the two unitary strokes that change the Hamiltonian of the system between $H^{(1)}$ and $H^{(2)}$, preserve the populations of the two-level system despite making the state diagonal on the eigenbasis of $H^{(1)}$ and $H^{(2)}$ respectively, in the adiabatic limit. Effectively, it is equivalent to the action of the Hadamard operation \mathcal{H} which performs the transformation of basis as follows: $\{|0\rangle, |1\rangle\} \rightarrow \{|+\rangle, |-\rangle\}$

and vice versa. In our context, $H^{(1)}$ and $H^{(2)}$ are given by

$$H^{(1)} = \frac{\hbar}{2}\omega_z\sigma_z = \frac{\hbar}{2}\omega_z(|0\rangle\langle 0| - |1\rangle\langle 1|), \text{ and} \quad (1)$$

$$H^{(2)} = \frac{\hbar}{2}\omega_x\sigma_x = \frac{\hbar}{2}\omega_x(|+\rangle\langle +| - |-\rangle\langle -|), \quad (2)$$

where \hbar denotes the reduced Planck constant. We note that $\mathcal{H}H^{(1)}\mathcal{H}^\dagger = \hbar\omega_z\sigma_x/2 = (\omega_z/\omega_x)H^{(2)}$, where \mathcal{H} is the Hadamard gate.

Now, let us calculate the work done in the first unitary stroke-II. The work done W_1 is given by the difference between the final and initial energy of the working medium, i.e.,

$$\begin{aligned} W_1^x &= E_1^x - E_0^x \\ &= \text{Tr}(H^{(2)}\rho_1^x) - \text{Tr}(H^{(1)}\rho_0^x) \\ &= \text{Tr}(H^{(2)}\rho_1^x) - \text{Tr}(H^{(1)}\mathcal{H}\rho_1^x\mathcal{H}) \\ &= \left(1 - \frac{\omega_z}{\omega_x}\right)E_1^x. \end{aligned} \quad (3)$$

Here, we have used the fact that under adiabatic unitary evolution in stroke-II, the probabilities of the two levels remain invariant but the two level change from the eigenbasis of $H^{(1)}$ to that of $H^{(2)}$, viz., $\rho_0^x = \mathcal{H}\rho_1^x\mathcal{H}$. Similarly, we have

$$W_2^x = E_3^x - E_2^x = -\left(1 - \frac{\omega_z}{\omega_x}\right)E_2^x$$

So, the total work W comes out to be,

$$W^x = -(W_1^x + W_2^x) = \left(1 - \frac{\omega_z}{\omega_x}\right)(E_2^x - E_1^x). \quad (4)$$

The heat absorbed Q_h is given by $Q_h^x = E_2^x - E_1^x$. Thus, the efficiency turns out to be,

$$\eta := \frac{W^x}{Q_h^x} = \left(1 - \frac{\omega_z}{\omega_x}\right). \quad (5)$$

We would like to reiterate that the efficiency of the otto engine remains independent of the nature of the process involved in stroke-III of the cycle, as is evident from Eq. (5). Thus, it is important to investigate whether the work output of the engine differs for different processes in stroke-III. Furthermore, in our later analysis, while considering POVM in stroke-III, we model this by introducing an additional auxiliary qubit, which along with the system-qubit, undergoes a unitary operation, followed by a PV measurement on the auxiliary qubit. In such a case, it is necessary to reset the auxiliary qubit after the current cycle, so that it can be reused in the next cycle. This qubit-reset may require additional work which can be provided from the net work W , in which case, the net work decreases, thereby reducing the efficiency. This can be prevented either by discarding the auxiliary qubit after every cycle and use a already prepared auxiliary qubit or by thermalizing the auxiliary qubit along with the work qubit during stroke-I.

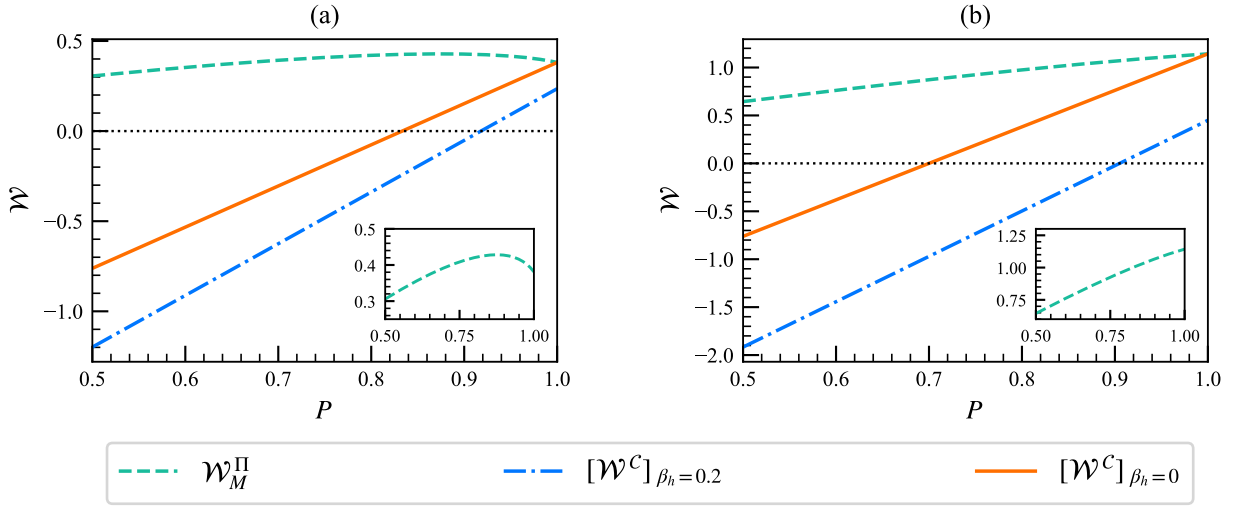


Figure 2. **Extractable work: comparison between the PVM-based and conventional two-bath Otto engines.** The non-adiabatic work output, \mathcal{W} , is plotted as a function of the non-adiabaticity parameter P , where $P = 1$ corresponds to the adiabatic limit. The dashed turquoise curve denotes the maximum extractable work from the PVM-based Otto engine, $\mathcal{W}_M^{\text{II}}$, obtained after optimization over all measurement settings. For comparison, the work extracted from a conventional two-bath Otto engine is also shown for two hot-bath inverse temperatures: $\beta_h = 0.2$ (dot-dashed blue) and $\beta_h = 0$ (solid orange), represented by $[\mathcal{W}^C]_{\beta_h=0.2}$ and $[\mathcal{W}^C]_{\beta_h=0}$, respectively. Panels (a) and (b) correspond to two different compression ratios, $\gamma = \omega_x/\omega_z$: (a) $\gamma = 1.5$ with $(\omega_x, \omega_z) = (3, 2)$, and (b) $\gamma = 2.5$ with $(\omega_x, \omega_z) = (5, 2)$. The dotted black line corresponds to $\mathcal{W} = 0$. Above this line, the cycle operates as an engine and delivers positive work output, whereas below it, the cycle absorbs work and therefore ceases to function as an engine. The insets show $\mathcal{W}_M^{\text{II}}$ separately in order to clearly illustrate its non-monotonic dependence on P in panel (a) and monotonic dependence in panel (b).

IV. PVM-FUELED QUANTUM OTTO ENGINES

In this section, we determine the optimal work extractable from a quantum Otto engine when stroke-III is replaced by a projective measurement, and identify the measurement basis that maximizes this extraction. We analyze two scenarios: one with adiabatic unitary strokes and another with non-adiabatic strokes.

A. Adiabatic PVM-fueled quantum Otto engine

We first consider the scenario with adiabatic unitary strokes. Strokes I and II are identical to those in the conventional Otto engine operating between two thermal baths (for complete analysis for traditional two bath engine, see Appendix. A). Consequently, the energies of the working substance after Strokes I and II, denoted by E_0^{II} and E_1^{II} , are the same as in the conventional Otto cycle. The energy corresponding to the states after stroke-I and stroke-II is

$$E_0^{\text{II}} = -\frac{\hbar}{2}\omega_z \tanh v_z, \quad \text{and} \quad (6)$$

$$E_1^{\text{II}} = -\frac{\hbar}{2}\omega_x \tanh v_z, \quad (7)$$

respectively. See Appendix. A for details. Accordingly, the work output during stroke-II, $W_1^{\text{II}} = E_1^{\text{II}} - E_0^{\text{II}}$ is given by

$$W_1^{\text{II}} = \frac{\hbar}{2} \tanh v_z (\omega_z - \omega_x). \quad (8)$$

We now consider stroke-III, where a projective (PV) measurement is performed. Without loss of generality, the measurement basis can be taken as $\{|\psi_{\theta\phi}^+\rangle, |\psi_{\theta\phi}^-\rangle\}$, where

$$\begin{aligned} |\psi_{\theta\phi}^+\rangle &:= \cos \frac{\theta_x}{2} |+\rangle + e^{i\phi_x} \sin \frac{\theta_x}{2} |-\rangle, \quad \text{and} \\ |\psi_{\theta\phi}^-\rangle &:= \sin \frac{\theta_x}{2} |+\rangle - e^{i\phi_x} \cos \frac{\theta_x}{2} |-\rangle. \end{aligned} \quad (9)$$

These two states are orthogonal, i.e., $\langle \psi_{\theta\phi}^+ | \psi_{\theta\phi}^- \rangle = 0$. Here, $\theta_x \in [0, \pi]$ and $\phi_x \in [0, 2\pi)$ denote the polar angle and the azimuthal angle, respectively, in the Bloch sphere representation of the qubit with two poles representing $|+\rangle$ and $|-\rangle$. We discard the outcome of the measurement, hence the post-measurement state comes out to be,

$$\rho_2^{\text{II}} = p_{\psi_{\theta\phi}^+} |\psi_{\theta\phi}^+\rangle \langle \psi_{\theta\phi}^+| + p_{\psi_{\theta\phi}^-} |\psi_{\theta\phi}^-\rangle \langle \psi_{\theta\phi}^-|,$$

where

$$p_{\psi_{\theta\phi}^\pm} = \langle \psi_{\theta\phi}^\pm | \rho_2 | \psi_{\theta\phi}^\pm \rangle = \frac{1}{2} (1 \mp \tau_z \cos \theta_x).$$

Here, $\tau_z := \tanh v_z$ and $p_{\psi_{\theta\phi}^+} + p_{\psi_{\theta\phi}^-} = 1$. Consequently, the energy of the qubit after stroke-III comes out to be,

$$E_2^{\text{II}} = \text{Tr}(H^{(2)} \rho_2) = -\frac{\hbar}{2} \omega_x \tau_z \cos^2 \theta_x. \quad (10)$$

The change in energy of the working substance in the stroke-III is attributed as heat absorbed by the working qubit. This heat absorbed, Q_h , due to the measurement stroke is given by

$$Q_h^{\text{II}} = E_2^{\text{II}} - E_1^{\text{II}} = \frac{\hbar}{2} \omega_x \tau_z \sin^2 \theta_x. \quad (11)$$

Finally, after the measurement stroke, we have the final work stroke. The stroke-IV, which is a unitary evolution induced by the adiabatic change of the qubit Hamiltonian from $H^{(2)}$ to $H^{(1)}$. This evolution, being adiabatic, preserves the elements of the density matrix, but the basis changes from the eigenbasis of $H^{(2)}$ to that of $H^{(1)}$. Hence, the state ρ_3^Π after stroke-IV is given by

$$\rho_3^\Pi = p_{++}|0\rangle\langle 0| + p_{+-}|0\rangle\langle 1| + p_{-+}|1\rangle\langle 0| + p_{--}|1\rangle\langle 1|,$$

and the corresponding energy E_3 is given by

$$E_3^\Pi = \text{Tr}(H^{(1)}\rho_3) = -\frac{\hbar}{2}\omega_z\tau_z\cos^2\theta_x.$$

Here, $\{p_{ij}\}_{i,j=\pm}$, which are the elements of ρ_2^Π in $\{|+\rangle, |-\rangle\}$ basis are given by $p_{++} = (1 - \tau_z\cos^2\theta_x)/2$, $p_{+-} = -e^{-i\phi_x}\tau_z\sin(2\theta_x)/4$, $p_{-+} = p_{+-}^*$, and $p_{--} = (1 + p_{++})$. The work done associated with this stroke is evaluated to be

$$W_2^\Pi = E_3^\Pi - E_2^\Pi = \frac{\hbar}{2}(\omega_x - \omega_z)\tau_z\cos^2\theta_x. \quad (12)$$

Finally, the qubit undergoes thermalizing stroke-I, and gets reset to the thermal state, corresponding to the temperature T_c . The heat given out by the qubit in this stroke is given by

$$Q_c^\Pi = E_0^\Pi - E_3^\Pi = -\frac{\hbar}{2}\omega_z\tau_z\sin^2\theta_x.$$

With the help of Eq. (8), according to the convention discussed in subsection II C the total work comes out to be,

$$W^\Pi = -(W_1^\Pi + W_2^\Pi) = \frac{\hbar}{2}\tau_z(\omega_x - \omega_z)\sin^2\theta_x. \quad (13)$$

For $\omega_z < \omega_x$, the work output by the engine, W^Π is positive, indicating that the engine operates in the work-producing regime. Furthermore, we note that $Q_h^\Pi + Q_c^\Pi = W^\Pi$, signifying that the total energy in the cyclic process is conserved, satisfying the first law of thermodynamics.

We find that the efficiency of the PVM-based engine is given by $\eta^\Pi = \frac{W^\Pi}{Q_h^\Pi} = 1 - (\omega_z/\omega_x)$, which matches with the expression obtained in Eq. (5) for more general settings.

From Eq. (13), we find that the total work output is maximized for $\theta_x = \pi/2$, which corresponds to the measurement basis of $\{|0\rangle, |1\rangle\}$, i.e., the computational basis. The corresponding maximum value is given by

$$W_M^\Pi = \frac{\hbar}{2}\tau_z(\omega_x - \omega_z), \quad (14)$$

where the maximization is over the set of all PV-measurements. In Appendix. A, we show that a conventional Otto cycle operating with a hot bath with infinite temperature ($\beta_h = 0$), produces the maximum work $W_M^C = (\hbar/2)\tau_z(\omega_x - \omega_z)$. This is identical to the maximum work, W_M^Π obtained by the PVM-based Otto engine, with same parameters. Thus, in the realistic scenario, where the hot bath has finite-temperature $\beta_h > 0$, the PVM-based Otto engine produces more work than the traditional one.

B. Non-adiabatic PVM-fueled quantum Otto engine

In this subsection, we consider non-adiabatic work strokes in PVM-based Otto engine. The stroke-II and IV are unitary strokes, where the Hamiltonian of the qubit working substance changes with time. Thus, the unitary operation U acting on the state in such a stroke is given by

$$U = \mathcal{T} \left[\exp \left(-\frac{i}{\hbar} \int_{t_1}^{t_2} H(t') dt' \right) \right], \quad (15)$$

where $H(t')$ is the time-dependent Hamiltonian, with U being acted on the system from time t_1 up to time t_2 , and \mathcal{T} denotes the time-ordering operator.

For a generic time-dependent Hamiltonian $H(t')$ that interpolates between $H^{(1)}$ and $H^{(2)}$, i.e., $H(t_1) = H^{(2)}$ and $H(t_2) = H^{(1)}$, the corresponding unitary evolution operator U can be written as

$$U|0\rangle = \sqrt{P}|+\rangle + e^{i\alpha}\sqrt{1-P}|-\rangle \quad (16)$$

$$\text{and } U|1\rangle = \sqrt{1-P}|+\rangle - e^{i\alpha}\sqrt{P}|-\rangle, \quad (17)$$

where the parameters P and α depend on the driving protocol $H(t)$ and the total evolution time. In the adiabatic limit, $P = 1$, whereas $P \in [1/2, 1)$ characterizes the non-adiabatic regime. The parameter P can be interpreted as the transition probability.

The matrix representation of U in the eigenbasis of σ_z is given by

$$U = \frac{1}{\sqrt{2}} \begin{pmatrix} \sqrt{P} + e^{i\alpha}\sqrt{1-P} & \sqrt{1-P} - e^{i\alpha}\sqrt{P} \\ \sqrt{P} - e^{i\alpha}\sqrt{1-P} & \sqrt{1-P} + e^{i\alpha}\sqrt{P} \end{pmatrix},$$

where $\alpha \in [0, 2\pi)$. Let us now calculate the work given out by such a non-adiabatic PV-Otto engine. The thermalizing stroke-I is the same as in the conventional Otto engine. Therefore, the post thermalization-state $\tilde{\rho}_0^\Pi = \exp(-\beta_c H^{(1)})/\mathcal{Z}$ (see Eq. (A1)) and its corresponding energy $\mathcal{E}_0^\Pi = -(\hbar/2)\omega_z\tau_z$ (see Eq. (6)).

In the stroke-II, which is also the same as in the conventional Otto engine, the evolution of the system is given by the unitary U , such that $\tilde{\rho}_1^\Pi = U\tilde{\rho}_0^\Pi U^\dagger$, and its corresponding energy is given by

$$\mathcal{E}_1^\Pi = \frac{\hbar}{2}\omega_x\tau_z(1 - 2P), \quad (18)$$

which is identical to the conventional Otto cycle one, see Eq. (B2). Hence, the work in this stroke turns out to be

$$\begin{aligned} \mathcal{W}_1^\Pi &= \mathcal{E}_1^\Pi - \mathcal{E}_0^\Pi \\ &= \frac{\hbar}{2}\tau_z(\omega_x(1 - 2P) + \omega_z), \end{aligned} \quad (19)$$

In the next stroke, the system undergoes a PV measurement. Consequently, we have, $\tilde{\rho}_2^\Pi = p_{\psi_\theta^+}^{\text{na}} |\psi_\theta^+\rangle\langle\psi_\theta^+| + p_{\psi_\theta^-}^{\text{na}} |\psi_\theta^-\rangle\langle\psi_\theta^-|$. Consequently, the energy of $\tilde{\rho}_2^\Pi$ is

$$\mathcal{E}_2^\Pi = \text{Tr}(H^{(2)}\rho_2) = -\frac{\hbar}{2}\omega_x\tau_z(2B - 1)(2A - 1), \quad (20)$$

where $B := |\langle \psi_{\theta\phi}^+ | + \rangle|^2$ and $A := |\langle \psi_{\theta\phi}^+ | U | 0 \rangle|^2$ (see Appendix C for detailed derivation). Hence, the amount of injected heat in the system, by the measurement stroke is given by

$$\begin{aligned} Q_h^\Pi &= \mathcal{E}_2^\Pi - \mathcal{E}_1^\Pi \\ &= -\frac{\hbar}{2}\omega_x\tau_z [(2B-1)(2A-1) + (1-2P)] \end{aligned} \quad (21)$$

The measurement stroke is followed by another non-adiabatic unitary stroke-IV. The unitary \tilde{U} governing this stroke, emerges from a driven Hamiltonian, that initially is $H^{(2)}$ and at the end becomes $H^{(1)}$. The unitary \tilde{U} is of the form similar to that of Eq. (15). The unitary-evolved state is $\tilde{\rho}_3^\Pi = \tilde{U}\rho_2\tilde{U}^\dagger$ and the corresponding energy is

$$\mathcal{E}_3^\Pi = -\frac{\hbar}{2}\omega_z\tau_z(2Q-1)(2A-1), \quad (22)$$

where $Q := |\langle 0 | \tilde{U} | \psi_{\theta\phi}^+ \rangle|^2$. See Appendix C for further details.

From Eq. (22) and Eq. (20), we obtain the work associated with stroke-IV as

$$\begin{aligned} \mathcal{W}_2^\Pi &= \mathcal{E}_3^\Pi - \mathcal{E}_2^\Pi \\ &= \frac{\hbar}{2}\tau_z(2A-1) [\omega_x(2B-1) - \omega_z(2Q-1)]. \end{aligned} \quad (23)$$

From Eq. (19) and Eq. (23), we obtain the total work as

$$\begin{aligned} \mathcal{W}^\Pi &= -(\mathcal{W}_1^\Pi + \mathcal{W}_2^\Pi) \\ &= -\frac{\hbar}{2}\tau_z [(\omega_x(1-2P) + \omega_z) \\ &\quad + (2A-1)(\omega_x(2B-1) - \omega_z(2Q-1))]. \end{aligned} \quad (24)$$

The qubit is reset to the Gibbs state of $\tilde{\rho}_0^\Pi$ in the thermalizing (to the cold-bath) stroke-I, thereby starting the cycle again. The amount of exchanged heat with the cold-bath is given by

$$\begin{aligned} Q_c^\Pi &= \mathcal{E}_0^\Pi - \mathcal{E}_3^\Pi \\ &= -\frac{\hbar\tau_z}{2}\omega_z(1 + (2Q-1)(2A-1)) \end{aligned} \quad (25)$$

Again, we find that $Q_h^\Pi + Q_c^\Pi = \mathcal{W}^\Pi$, thus satisfying the first law of thermodynamics.

We have considered quite a general \tilde{U} for the stroke-IV up to this point. In order to simplify our analysis, from this point onward we consider the two unitary strokes to be symmetric. Thus, for the Otto cycle, the unitary \tilde{U} of the stroke-IV retraces the exact path of U of stroke-II reversibly. Consequently, we obtain $\tilde{U} = U^\dagger$, where $\tilde{U} = \mathcal{T} \left[\exp \left(-\frac{i}{\hbar} \int_{t_1}^{t_2} \tilde{H}(t') dt' \right) \right]$ with $\tilde{H}(t') = H(t_2 + t_1 - t')$ [55]. With this consideration, we have $Q = |\langle 0 | U^\dagger | \psi_{\theta\phi}^+ \rangle|^2 = |\langle \psi_{\theta\phi}^+ | U | 0 \rangle|^2 = A$.

Now, let us optimize W for a given set of P and α . Expressing $|\psi\rangle$ in the Bloch sphere representation as $|\psi\rangle = \cos(\theta_x/2)|+\rangle + e^{i\phi_x}\sin(\theta_x/2)|-\rangle$, we obtain $2A-1 = (2P-1)\cos\theta_x + 2\sqrt{P(1-P)}\sin\theta_x\cos(\alpha-\phi_x)$ and $2B-1 = \cos\theta_x$.

Now, from Eq. (24), the total work can be rewritten as

$$\mathcal{W}^\Pi = -\frac{\hbar\tau_z}{2}[-a\omega_x + \omega_z - \omega_z\mu^2 + \omega_x\mu\cos\theta_x], \quad (26)$$

where $a := 2P-1$, $b := 2\sqrt{P(1-P)}$, and $\mu := a\cos\theta_x + b\sin\theta_x\cos(\alpha-\phi_x)$.

Here, we analytically optimize over θ and ϕ for a given set of α and P . The explicit optimization and analysis are shown in Appendix E. The optimal work for a given set of α and P is given by

$$\begin{aligned} \mathcal{W}_M^\Pi &= \frac{\hbar\tau_z}{4} (\sqrt{(\omega_x - \omega_z)^2 + 4\omega_x\omega_z(1-P)} - \omega_z \\ &\quad + \omega_x(2P-1)), \end{aligned} \quad (27)$$

where the maximization is performed over the set of all PV-measurements.

Behavior of the Otto cycle based on the compression ratio.

Here, we focus on the maximization of \mathcal{W}^Π over the set of the non-adiabaticity parameter, i.e., $P \in [1/2, 1]$. We observe that the maximization behaves differently in the two distinct regimes of the compression ratio $\gamma := \omega_x/\omega_z$. For $\gamma < 2$, optimal work is extracted at the particular value of $P = P_0$, where,

$$P_0 := \frac{1}{2} + \frac{\omega_x}{4\omega_z} \quad (\gamma < 2),$$

and interestingly, this particular value of P lies in the strictly non-adiabatic region because $P_0 \in (1/2, 1)$. This optimal value of work is given by

$$[\mathcal{W}_M^\Pi]_{P=P_0} = \frac{\hbar\omega_x^2\tau_z}{8\omega_z}. \quad (28)$$

On the other hand, when $\gamma \geq 2$, optimal work is extracted particularly at $P_0 = 1$, which strictly represents the adiabatic limit. This optimal value of work is given by

$$[\mathcal{W}_M^\Pi]_{P=1} = \frac{\hbar\tau_z}{2}(\omega_x - \omega_z) \quad (29)$$

which coincides with Eq. (14).

PVM-based Otto cycle operates as an engine for the entire range of transition probabilities P . In contrast to the conventional Otto cycle, which fails to operate as an engine for certain values of the transition probability $P \in [1/2, 1]$, we find from Eq. (27) that $\mathcal{W}_M^\Pi > 0$ throughout this entire range. Hence, the PVM-based Otto cycle functions as an engine for all values of P .

This behavior is illustrated in Fig. 2, where we show the variation of the optimal extracted work with the transition probability P . The quantities $[\mathcal{W}^C]\beta_h = 0.2$ (blue dash-dotted), $[\mathcal{W}^C]\beta_h = 0$ (orange solid), and \mathcal{W}_M^Π (turquoise dashed) correspond to Eq. (B11), Eq. (B13), and Eq. (27), respectively. The blue dash-dotted and orange solid curves denote the extractable work of the conventional Otto cycle for $\beta_h = 0.2$ and $\beta_h = 0$, respectively, whereas the turquoise dashed curve corresponds to the PVM-based Otto cycle. Panel (a) corresponds to the regime $\gamma < 2$, obtained for

$\omega_x = 3$ and $\omega_z = 2$, giving $\gamma = 3/2$. Panel (b) corresponds to $\gamma > 2$, where $\omega_x = 5$ and $\omega_z = 2$, yielding $\gamma = 5/2$. In both panels, the inset provides a magnified view of W^Π within the relevant parameter regime. Fig.2 clearly demonstrates that, for the PVM-based Otto cycle, the extracted work remains positive over the entire range of P , as shown by the turquoise dashed curves. In contrast, the conventional Otto cycle with two thermal baths fails to maintain positive work extraction throughout the whole domain of P .

Efficiency at optimal work extraction. The efficiency $\eta_{\text{na}}^\Pi := \mathcal{W}_M^\Pi / \mathcal{Q}_h^\Pi$ for any given value of P is given by Eq. (F2) (for details, see Appendix F), i.e.,

$$\eta_{\text{na}}^\Pi = \frac{D(D + a\omega_x - \omega_z)}{\omega_x(a(D - (4a^2 - 3)\omega_z) + 8(P - 1)P\omega_x + \omega_x)}.$$

Here, we analyze the efficiency of the PVM-based Otto cycle when operated at optimal work extraction. For $\gamma \geq 2$, the optimal work extraction occurs in the adiabatic limit, corresponding to $P = 1$. In this regime, the efficiency is given by

$$[\eta_{\text{na}}^\Pi]_{P=1} = \eta^\Pi = 1 - \frac{\omega_z}{\omega_x}. \quad (30)$$

For $\gamma < 2$, the optimal work is extracted at $P = P_0$, consequently the efficiency is given by

$$[\eta_{\text{na}}^\Pi]_{P=P_0} = \frac{1}{2}. \quad (31)$$

For setups satisfying $\gamma < 2$, the efficiency at optimal work extraction is given by $1/2$, which is greater than the efficiency of the corresponding adiabatic engine, $\eta^\Pi = 1 - \frac{\omega_z}{\omega_x}$. Therefore, in this regime, $[\eta_{\text{na}}^\Pi]_{P=P_0} > \eta^\Pi$. Hence, for $\gamma < 2$, the transition probability $P = P_0$ not only yields more work extraction but also provides a higher efficiency than that of the adiabatic engine.

V. POVM-FUELED QUANTUM OTTO ENGINES

In this section, we consider a two-outcome POVM in the measurement stroke-III of the Otto engine. To realize the two-outcome POVM in the measurement stroke, we introduce an auxiliary system, initially in the state ρ_a . According to Naimark's dilation theorem, to implement a general two-outcome POVM, a global unitary operation is applied on the joint system-auxiliary state, and subsequently a PV measurement is applied on the auxiliary. In accordance to this, we act a global unitary operation V on the composite state $\rho_{sa} = \rho_1^P \otimes \rho_a$, and then perform a PV measurement on the composite system, of the form $\{I \otimes \Pi_i\}_i$, where I denotes the identity operator on the system, and $\{\Pi_i\}_{i=1,2}$ denote rank-one projectors on the auxiliary system. Following the completion of the measurement stroke, we decouple the auxiliary system. The bipartite state after the completion of the measurement stroke-III, without post-selection, is given by

$$\rho'_{sa} = \sum_{i=1}^2 (I \otimes \Pi_i)(V\rho_{sa}V^\dagger)(I \otimes \Pi_i). \quad (32)$$

Furthermore, we consider the unitary strokes to be either adiabatic or non-adiabatic.

A. Adiabatic POVM-fueled quantum Otto engine

As discussed in the previous sections, in measurement-based Otto engines, strokes I and II are the same as in the conventional two-bath Otto engine. Thus, we have $E_0^P = (-\hbar/2)\omega_z\tau_z$ and $E_1^P = (-\hbar/2)\omega_x\tau_z$, consequently work output in the stroke-II is

$$W_1^P = (\hbar/2)\tau_z(\omega_z - \omega_x)$$

In stroke-III, the POVM-stroke of the engine, the final system-auxiliary state is given by ρ'_{sa} (Eq. (32)). Here, we can assume that the auxiliary has a trivial Hamiltonian; any change in its state does not have an energy cost. The energy of the system after the measurement stroke is

$$E_2^P = \text{Tr} \left[(H^{(2)} \otimes I)(V\rho_{sa}V^\dagger) \right]. \quad (33)$$

The details are given in Appendix G. In stroke-IV, the Hamiltonian is adiabatically varied from $H^{(2)}$ to $H^{(1)}$. Under this adiabatic evolution, the density matrix remains invariant in the instantaneous eigenbasis $\{|+\rangle, |-\rangle\}$, while the basis itself is continuously transformed into the computational basis. Consequently, the state transforms as $\rho_3^P = \mathcal{H}\rho_2^P\mathcal{H}$, with $\rho_2^P = \text{Tr}_a[\rho'_{sa}]$. Thus, the corresponding energy of the engine after the stroke-IV is $E_3^P = \text{Tr}[H^{(1)}\rho_3^P] = (\omega_z/\omega_x)E_2^P$. Thus, the total work done by the engine turns out to be

$$W^P = \left(1 - \frac{\omega_z}{\omega_x}\right) \left(E_2^P + \frac{\hbar}{2}\omega_x\tau_z\right). \quad (34)$$

In order to find the maximum work extractable from the engine, we require the maximization of E_2^P . This maximization can be analytically obtainable by arranging the eigenvalues of $H^{(2)} \otimes I$ and $V\rho_{sa}V^\dagger$, denoted by, say r_i and s_i , respectively. The maximum value comes out to be $\sum_i r_i^\uparrow s_i^\uparrow$, where r_i^\uparrow and s_i^\uparrow are obtained by arranging r_i and s_i , respectively in the ascending order.

Let us now, maximize the energy E_2^P over all possible two-outcome POVM measurements. For this let us first consider the initial state of the auxiliary system as a pure state. The analysis with initially mixed auxiliary state is presented in Appendix I. We note that the maximum work is obtained from the set of POVM realized using initially pure auxiliary state. The pure qubit auxiliary state has the eigenvalues of 1 and 0. Moreover, the two eigenvalues of ρ_1 are $\exp(-v_z)/\mathcal{Z}$ and $\exp(v_z)/\mathcal{Z}$, where $\mathcal{Z} = 2 \cosh v_z$. Thus, we obtain the eigenvalues of ρ_{sa} in ascending order as $\{s_i^\uparrow\} = \{\exp(v_z)/\mathcal{Z}, \exp(-v_z)/\mathcal{Z}, 0, 0\}$. Similarly, the eigenvalues of $H^{(2)} \otimes I$ in ascending order turns out to be $\{r_i^\uparrow\} = \{(\hbar/2)\omega_x, (\hbar/2)\omega_x, -(\hbar/2)\omega_x, -(\hbar/2)\omega_x\}$.

Thus we can obtain the maximum value of E_2^P as

$$\left[E_2^P\right]_M = \sum_i r_i^\uparrow s_i^\uparrow = \frac{\hbar}{2}\omega_x. \quad (35)$$

This leads to the maximum work extractable from the engine to be

$$W_M^P = \frac{\hbar}{2}(\omega_x - \omega_z)(1 + \tau_z), \quad (36)$$

where the maximization is performed over the set of all two-outcome POVMs. After the completion of the measurement stroke, the system undergoes a unitary stroke-IV and finally followed by a thermalizing stroke to reset the working qubit to start another cycle. To analyze further we need to find the post-measurement state ρ_2^P of the system.

Feasibility of the optimal work: Having derived the optimal work extractable from the POVM-based Otto engine, W_M^P (Eq. (36)), a natural question is whether this optimum can be achieved, and if so, which specific POVM realizes it. To find the POVM that optimizes work, we need to find a unitary operator V_0 , which maximizes the energy E_2^P . We note that $\text{supp}(\rho_{sa}) = \mathbb{S}_{sa} = \{|+\rangle, |-\rangle\}$, but the energy operator $H^{(2)} \otimes I$, has $\mathbb{S}_{h^{(2)}} = \{|+\rangle, |+\rangle\}$ as a higher energy subspace. Thus a unitary that takes the state from $\mathbb{S}_{sa} \rightarrow \mathbb{S}_{h^{(2)}}$ leads to optimal work.

One such unitary operator V_0 , which can be expressed as a permutation matrix is given by

$$V_0 = \begin{pmatrix} 1 & 0 & 0 & 0 \\ 0 & 0 & 1 & 0 \\ 0 & 1 & 0 & 0 \\ 0 & 0 & 0 & 1 \end{pmatrix}, \quad (37)$$

in matrix representation on the eigen-basis of σ_x . Now, let find the effect of the POVM on the system. Following the joint evolution with V , the local PV measurement is performed on the auxiliary in the basis $\{\Pi_i\} = \{|\psi_{\theta\phi}^+\rangle\langle\psi_{\theta\phi}^+|, |\psi_{\theta\phi}^-\rangle\langle\psi_{\theta\phi}^-|\}$, where $|\psi_{\theta\phi}^+\rangle$ and $|\psi_{\theta\phi}^-\rangle$ are given by Eq. (9). The post-measurement state becomes $\rho_2^P = \sum_{i=+,-} K_i \rho_1 K_i^\dagger$, where $K_+ = {}_a\langle\psi_{\theta\phi}^+|V_0|+\rangle_a$ and $K_- = {}_a\langle\psi_{\theta\phi}^-|V_0|+\rangle_a$, with $K_+^\dagger K_+ + K_-^\dagger K_- = I$. Thus, we obtain the post-measurement state of the system to be $\rho_2^P = \text{Tr}_a(\rho'_{sa}) = |+\rangle\langle+|$, which yields $E_2 = \text{Tr}(\rho_2 H^{(2)}) = \hbar\omega_x/2$. Following the measurement in stroke-III, the system is adiabatically evolved by driving the Hamiltonian from $H^{(2)}$ to $H^{(1)}$. Hence, we have $\rho_3^P = |0\rangle\langle 0|$ and $E_3^P = (\hbar/2)\omega_z$. We evaluate the total work $W_M^P = (\hbar/2)(\omega_x - \omega_z)(1 + \tau_z)$, which is identical to the optimal extracted work from a POVM-based Otto engine. These expressions match with the ones we derived at the beginning of the section without explicitly finding out the state of the engine at intermediate points between each strokes.

Moreover, we would like to reiterate that V_0 is not a unique unitary operation that optimizes the work. It can be said that any unitary operation which maps the support set of ρ_{sa} , \mathbb{S}_{sa} to the highest energy subspace $\mathbb{S}_{h^{(2)}}$, can serve as the optimal unitary in this scenario. For a more detailed analysis on this, see Appendix H.

B. Non-adiabatic POVM-fueled quantum Otto engine

We now consider the POVM-based engine with non-adiabatic work strokes. Here, we numerically maximize the

extractable work over all two-outcome POVM measurements to obtain W_M^P . Specifically, for a given value of the transition probability P , we optimize the extractable work with respect to the system-auxiliary joint unitary operator V appearing in Eq. (32). In this analysis, for convenience, we set the parameter $\alpha = 0$ of the unitary work stroke U in Eq. (17).

The global unitary operator V acts on a four-dimensional Hilbert space and therefore possesses $4^2 - 1 = 15$ independent real parameters, since $V \in SU(4)$. We parametrize it as

$$V = \exp\left(i \sum_{j=1}^{15} k_j g_j\right), \quad (38)$$

where $k_j \in \mathbb{R}$ and $g_j \in \mathbb{G}$ for all $j \in \{1, \dots, 15\}$. Here, \mathbb{G} denotes the set of generators of $SU(4)$, $\mathbb{G} = \{\sigma_i \otimes \sigma_j, \sigma_i \otimes I, I \otimes \sigma_i \mid i, j = x, y, z\}$. During the numerical optimization, we fix the measurement basis as $\{\Pi_i\} = \{|+\rangle\langle+|, |-\rangle\langle-|\}$, since optimization over the 15 parameters of the unitary operator V alone is sufficient to span the entire set of two-outcome POVMs. The numerical optimization is performed using the ‘‘dual annealing’’ global optimization algorithm from SciPy, followed by a local optimization routine.

The numerically optimized maximum extractable work W_M^P (turquoise dashed) as a function of the non-adiabaticity parameter P is shown in Fig. 3, where $P = 1$ corresponds to the adiabatic limit. Panels (a) and (b) correspond to the regimes $\gamma < 2$ and $\gamma \geq 2$, respectively. At the adiabatic limit ($P = 1$), this curve coincides with the analytical value given by Eq. (36), shown by the yellow dotted horizontal line, thereby confirming the consistency of the numerical optimization.

C. Incorporation of the auxiliary resetting cost

In our analysis of POVM-based Otto engine, we have considered an auxiliary system that is introduced in a pure state of $|+\rangle$ in every cycle. The analysis up to now has considered a supply of the initially pure auxiliary enough for the number cycles for which the engine will be run. This could be a difficult condition to meet. Hence, here we consider the cost of recycling the auxiliary system after each cycle. In other words, the auxiliary is reset to a specific pure state after each cycle. This is similar to the case of Landauer’s principle [82–84], where a system in any state is erased to a specific pure state. According to the Landauer’s principle, any process that erases a state σ_{er} to a specific pure state $|\psi_{\text{erased}}\rangle$, requires at least $k_B T S(\sigma_{\text{er}}) \ln 2$, and this energy is released to the environment as heat. Here, k_B is the Boltzmann constant, T is temperature of the surrounding, $S(\sigma_{\text{er}})$ is the von-Neumann entropy of the state σ_{er} to be erased.

We find that the auxiliary after the measurement stroke is in some mixed state, ρ'_a . The auxiliary is erased to the pure state of $|+\rangle$ while being in contact with the cold-bath with temperature T_c . So, the erasure cost of for recycling the auxiliary is $W_a = k_B T_c S(\rho'_a) \ln 2$. It is essential to remove this amount of work from the total work output of the POVM-based Otto engine. In the next section, we discuss when this net work

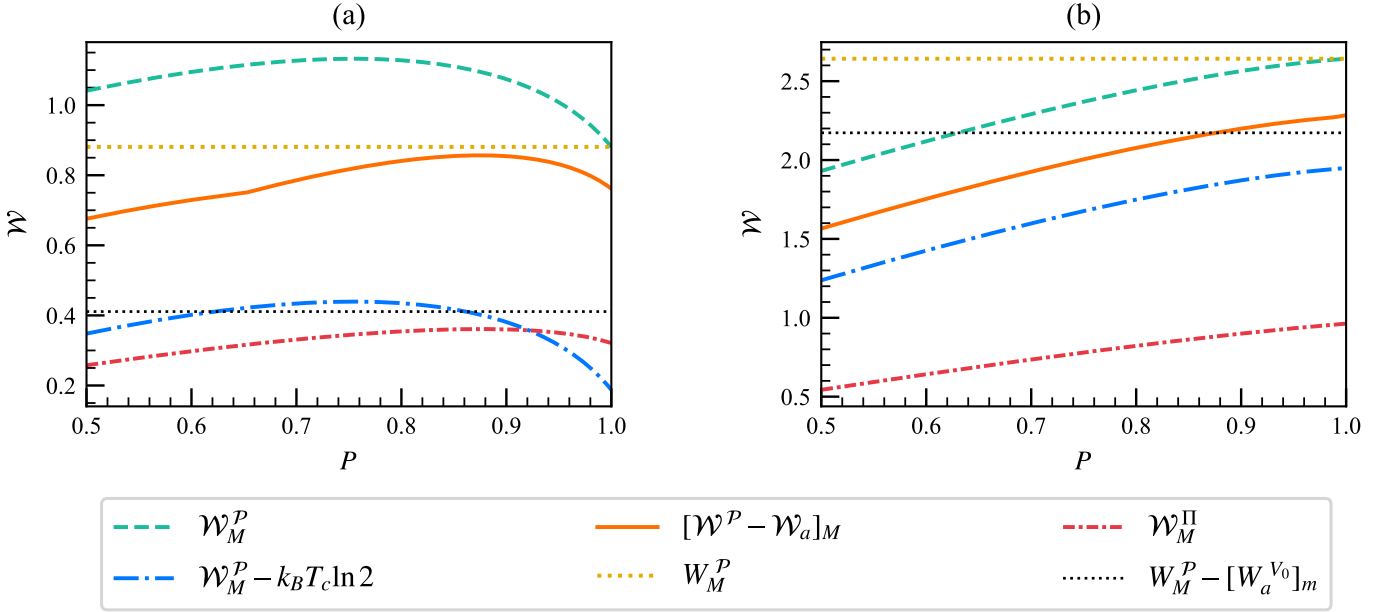


Figure 3. **Extractable work: comparison between the PVM-based and POVM-based Otto engines.** The non-adiabatic work output, \mathcal{W} , is plotted as a function of the non-adiabaticity parameter P , where $P = 1$ corresponds to the adiabatic limit. The turquoise dashed curve denotes the maximum extractable work from the POVM-based Otto engine, \mathcal{W}_M^P , obtained after optimization over all measurement settings. At the adiabatic limit, i.e., $P = 1$, this curve touches with the analytically derived value, i.e., W_M^P , represented by the yellow-colored dotted horizontal line. The lower bound on the net work extractable from the optimal POVM-based Otto engine, after accounting for the auxiliary reset cost, is obtained by subtracting the maximum auxiliary erasure cost, $k_B T_c \ln 2$, from \mathcal{W}_M^P . This lower bound is represented by the blue long dash-dotted curve. The numerical optimization over the net work $[\mathcal{W} - \mathcal{W}_a]_M$ is illustrated by the orange solid curve. The horizontal black-dotted line shows the optimal net work $W_M^P - W_a^{V_0}$, according to Eq. (45). For comparison, the optimal work extracted from a PVM-based Otto engine is also shown (red tiny dot-dash), represented by $\mathcal{W}_M^{\text{II}}$. Panels (a) and (b) correspond to two different compression ratios, $\gamma = \omega_x/\omega_z$: (a) $\gamma = 1.5$ with $(\omega_x, \omega_z) = (3, 2)$, and (b) $\gamma = 2.5$ with $(\omega_x, \omega_z) = (5, 2)$.

output from a POVM is larger than the corresponding PVM and two-bath cases.

Furthermore, Eq. (36) remains valid even when the auxiliary system is initialized in a pure state of a d -dimensional Hilbert space, characterized by a single nonzero eigenvalue equal to 1 and a $(d - 1)$ -fold degenerate zero eigenvalue, provided the optimization is performed over all d -outcome POVMs. In this more general setting, the maximum erasure cost associated with recycling the auxiliary system is bounded by $k_B T_c \ln d$. Nevertheless, throughout the present work, we restrict our analysis to the case of a qubit auxiliary system.

VI. OPTIMAL WORK EXTRACTION: COMPARISON OF TWO-BATH, PVM-, AND POVM-BASED OTTO ENGINES

In this section, we compare the maximal work output of the three different kinds of Otto engine, discussed in this work. We present a summary of our discussions in tabular form in Table I.

A. Two-bath vs. PVM-based Otto engines

We compare the maximum work output from a PVM-based and two-bath conventional Otto engines. We consider both the

adiabatic and non-adiabatic unitary work strokes.

1. Comparison for the adiabatic implementation

The work output of a conventional two-bath Otto engine is given by $W^C = (\hbar/2)(\tau_z - \tau_x)(\omega_x - \omega_z)$, (see Eq. (A9)) where $\tau_x = \tanh[(\hbar/2)\beta_h \omega_x]$.

The work output is maximized in the limit $\beta_h \rightarrow 0$, corresponding to an infinitely hot bath, yielding $W_M^C = [W^C]_{\beta_h=0} = \frac{\hbar}{2}\tau_z(\omega_x - \omega_z)$. This coincides exactly with the maximal work output of the PVM-based Otto engine, i.e.,

$$W_M^C = W_M^{\text{II}}. \quad (39)$$

However, it is important to note that achieving this maximal work output in the conventional two-bath Otto engine requires the hot bath to be at infinite temperature. Since such a limit is physically unattainable, the PVM-based Otto engine offers an operational advantage by attaining the same maximal work output without requiring an infinitely hot reservoir.

2. Comparison for the non-adiabatic implementation

In the regime of non-adiabatic work strokes, the work output of the two-bath conventional Otto engine, after maximiz-

	Conventional two-bath [Ref. [55]]	PVM-based	POVM-based
Efficiency (adiabatic)	$\eta^C = \eta_0$ [Sec. III]	$\eta^\Pi = \eta_0$ [Sec. III]	$\eta^P = \eta_0$ [Sec. III]
Optimal work (adiabatic)	$W_M^C = \frac{\hbar}{2} \Delta\omega \Delta\tau$ [Eq.(A9)]	$\leq W_M^\Pi = \frac{\hbar}{2} \Delta\omega \tau_z$ [Eq. (14)]	$< W_M^P = \frac{\hbar}{2} \Delta\omega (1 + \tau_z)$ [Eq. (36)]
Optimal work (non-adiabatic)	$W_M^C = \frac{\hbar}{2} (\tau_z \omega_{xz}^a + \tau_x \omega_{zx}^a)$ [Eq. (B11)]	$< W_M^\Pi = \frac{\hbar}{4} \tau_z (D - \omega_{xz}^a)$ [Eq. (27)]	$<$ Numerically studied [Fig. 3]
Efficiency at optimal work extraction	$\eta_{na}^C = \eta^C = \eta_0$ [App. B]	$\eta_{na}^\Pi = \eta_0$ ($\gamma \geq 2$) [Eq. (30)] $\eta_{na}^\Pi = 1/2$ ($\gamma < 2$) [Eq. (31)]	$\eta^P = \eta_0$ ($\gamma \geq 2$) (adiabatic)

Table I. *Comparison between conventional two-bath, PVM-based, and POVM-based Otto engines.* The table summarizes the efficiencies and optimal work extraction for the three classes of quantum Otto engines in both adiabatic and non-adiabatic regimes. In the adiabatic limit, all three engines attain the same efficiency, η_0 . However, their maximum extractable works satisfy the hierarchy $W_M^C \leq W_M^\Pi < W_M^P$, where the equality holds only with the infinite-temperature hot bath in the conventional Otto cycle, i.e., $\beta_h = 0$. In the non-adiabatic regime, the corresponding optimized works also exhibit the ordering $W_M^C < W_M^\Pi < W_M^P$, where the POVM-based case has been analyzed numerically. Focusing on the maximization on the non-adiabaticity parameter P in case of the non-adiabatic regime of the PVM-based engine, the maximum work is obtained at $P_0 = (1/2) + (\omega_x/4\omega_z)$ when $\gamma < 2$ and in the adiabatic limit ($P = 1$) when $\gamma < 2$, with corresponding values given by Eq. (28) and Eq. (14), respectively. For the two-bath case, the maximization is over the temperature of the hot-bath, while for the other it is on the measurement setting, while keeping the temperature of the cold bath the same in all the engines. The results shown here for the POVM-based engine, do not consider the work cost associated with resetting the auxiliary. Such an analysis is undertaken in Sec. V and VI. The table further compares the efficiencies at optimal work extraction and lists the relevant analytical expressions. Here, $\eta_0 := 1 - (\omega_z/\omega_x)$, $D := \sqrt{(\omega_x - \omega_z)^2 + 4(1 - P)\omega_x\omega_z}$, $a := 2P - 1$, $\Delta\omega := \omega_x - \omega_z$, $\Delta\tau := \tau_z - \tau_x$, $\omega_{xz}^a := (\omega_x a - \omega_z)$, and $\omega_{zx}^a := (\omega_z a - \omega_x)$.

ing over the temperature of the hot bath, is given by

$$\mathcal{W}_M^C = \frac{\hbar}{2} \tau_z [(\omega_x(2P - 1) - \omega_z)],$$

as shown in Eq. (B13). From Eq. (27), we know that

$$\mathcal{W}_M^\Pi = \frac{\hbar}{4} \tau_z \left[\sqrt{\Delta\omega^2 + 4\omega_x\omega_z(1 - P)} - \omega_z + \omega_x(2P - 1) \right],$$

where $\Delta\omega := \omega_x - \omega_z$. Subtracting \mathcal{W}_M^C from \mathcal{W}_M^Π , we obtain

$$\begin{aligned} \Delta\mathcal{W}^{\Pi C} &:= \mathcal{W}_M^\Pi - \mathcal{W}_M^C \\ &= \frac{\hbar}{4} \tau_z [D - \Delta\omega + 2\omega_x(1 - P)], \end{aligned} \quad (40)$$

where $D := \sqrt{\Delta\omega^2 + 4\omega_x\omega_z(1 - P)}$.

We can clearly see that $D \geq \Delta\omega$, thus we have $\Delta\mathcal{W}^{\Pi C} \geq 0$, with equality holding for $P = 1$. Thus, in the non-adiabatic work stroke regime, the PVM-based engine provides more work output than the conventional two-bath Otto engine.

In Fig. 2 we present the change in \mathcal{W}_M^C (turquoise-dashed line) and \mathcal{W}_M^Π (orange-solid line) with change in non-adiabatic parameter P . We confirm that $\Delta\mathcal{W}_M^{PV-2b} \geq 0$, in other words, $\mathcal{W}_M^\Pi \geq \mathcal{W}_M^C$, with the equality attained at $P = 1$. We also observe that for compression ration $\gamma = \omega_x/\omega_z > 2$, the value of P , corresponding to maximum work output is $[P_{\mathcal{W}_M^\Pi}^\gamma]_{\gamma \geq 2} = 1$, where as for $\gamma < 2$, we have $[P_{\mathcal{W}_M^\Pi}^\gamma]_{\gamma < 2} = (2 + \gamma)/4$. We present this in Fig. 2(a), where we have set $\gamma = 3/2$, while in Fig. 2(b), we have set $\gamma = 5/2$.

B. PVM-based vs. POVM-based Otto engines

1. Comparison for the adiabatic implementation

In Sec. V A, we have presented the optimal work for the POVM-based Otto engine W_M^P in Eq. (36). On the other hand, the optimal work for the PVM-based Otto engine W_M^Π is derived in Sec. IV A as Eq. (14). The difference between the two is given by

$$\begin{aligned} \Delta W^{P\Pi} &:= W_M^P - W_M^\Pi \\ &= \frac{\hbar}{2} (\omega_x - \omega_z). \end{aligned} \quad (41)$$

Since $\omega_x > \omega_z$, we have $W_M^P > W_M^\Pi$. Interestingly, $\Delta W^{P\Pi}$ is only dependent on ω_x and ω_z , and independent of β_c . Thus, when we have a sufficient number of initially pure auxiliary states required for the POVM, the work output of the POVM-based engine is always greater than that of the PVM-based engine.

Considering the auxiliary reset cost. Now let us consider the case where the auxiliary required for the POVM measurement is reused and hence is reset after every cycle. As discussed in Sec. V C, the cost of erasing the auxiliary qubit, which is in a state ρ'_a after the POVM stroke to a pure state, is given by $W_a = k_B T_c S(\rho'_a) \ln 2$, where $S(\sigma) = -\text{Tr}(\sigma \log_2 \sigma)$ is the von-Neumann entropy.

Temperature regime where the auxiliary-reset POVM Otto engine outperforms PVM-based engines. We now determine the regime of the cold-bath temperature T_c for which the POVM-based Otto engine, including the auxiliary-reset cost, yields a larger net work output than the PVM-based Otto engine. The required condition is $\Delta W_M^{P\Pi} > W_a$, which leads

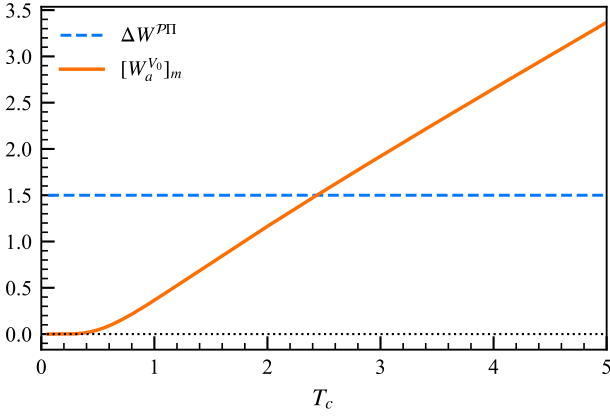


Figure 4. *Comparison between the advantage of the POVM-based engine over the PVM-based engine and the corresponding auxiliary reset cost.* The enhancement in work extraction offered by the POVM-based engine over the PVM-based engine is quantified by the difference between their respective optimal work outputs, $\Delta W^{P\Pi}$ [Eq. (41)], shown by the dashed blue curve. The solid orange curve represents the auxiliary reset cost, $[W_a^{V_0}]_m$ [Eq. (44)], associated with reinitializing the auxiliary system required for implementing the POVM. Both quantities are plotted as functions of the cold-bath temperature T_c . The results are shown for the compression ratio $\gamma = 2.5$, corresponding to $(\omega_x, \omega_z) = (5, 2)$.

to the bound

$$T_c < \frac{\hbar(\omega_x - \omega_z)}{2k_B \ln 2}.$$

In deriving this expression, we have used the inequality $S(\sigma) \leq 1$. We note that the entropy $S(\rho'_a)$ can, in general, depend on T_c through the joint state ρ'_{sa} . Incorporating this dependence results in a transcendental equation, yielding a tighter but analytically intractable bound. Therefore, we restrict ourselves to the simpler, weaker bound presented above.

Auxiliary-reset cost for POVM realized with joint unitary V_0 given in Eq. (37). The post-measurement without selection is obtained as the following: $\rho'_{sa} = \rho_2 \otimes \rho'_a$, with $\rho_2 = |+\rangle\langle+|$ and

$$\rho'_a = \begin{pmatrix} \nu^- & \lambda^- \\ \lambda^+ & \nu^+ \end{pmatrix}, \quad (42)$$

where $\nu^\pm := (1 \pm \tau_z \cos^2 \theta_x)/2$ and $\lambda^\pm := -e^{\pm i\phi_x} (\tau_z/4) \sin(2\theta_x)$ and ρ'_a is represented in the basis $\{|+\rangle, |-\rangle\}$ in Eq. (42). The von Neumann entropy of the post-measurement state of the auxiliary system ρ'_a is evaluated as

$$S(\rho'_a) = -(p_a^+ \log_2 p_a^+ + p_a^- \log_2 p_a^-), \quad (43)$$

where $p_a^\pm = (1 \pm \tau_z \cos \theta_x)/2$, where p_a^\pm are the eigenvalues of ρ'_a .

Minimum auxiliary-reset cost for POVM realized with joint unitary V_0 . We note from Eq. (43) that the auxiliary-reset cost depends on the measurement that is applied on the

auxiliary qubit following the V_0 unitary. But the work generated from the POVM-based Otto engine is independent of this measurement, see Eq. (36). Thus, we need to choose an appropriate PV measurement that minimizes the auxiliary-reset cost. We see that the choice of the PV measurement imprints on the final state ρ'_a of the auxiliary and thereby onto its entropy. The entropy is minimum when the value of p_a is far from $1/2$, which can be achieved by $\theta_x = 0$ or π . Hence, the measurement basis is to be chosen as $\{\Pi_i\} = \{|\pm\rangle\langle\pm|\}$ to minimize the auxiliary cost. The minimum auxiliary cost for POVM realized using the joint unitary V_0 of Eq. (37) is

$$[W_a^{V_0}]_m = -\frac{1}{2}k_B T_c (\ln 2) [t_z^+ \log_2(t_z^+/2) + t_z^- \log_2(t_z^-/2)], \quad (44)$$

where $t_z^\pm = 1 \pm \tau_z$. The net work output of the POVM-based Otto engine is obtained by subtracting the auxiliary cost from the optimized work given by Eq. (34). Thus, we obtain net work as

$$W_{\text{net}}^{V_0} = \frac{\hbar}{2}(\omega_x - \omega_z)(1 + \tau_z) - [W_a^{V_0}]_m. \quad (45)$$

Let us reiterate here that the maximum auxiliary-reset cost for the current case is $[W_a]_M = k_B T_c \ln 2$, obtained when $\theta_x = \pi/2$, i.e., $\{\Pi_i\} = \{|0\rangle\langle 0|, |1\rangle\langle 1|\}$.

Graphical visualization. In Fig. 4, we plot the difference between the optimal work extracted from the POVM-based and PVM-based Otto engines, $\Delta W^{P\Pi}$, shown by the blue dashed curve and given by Eq. (41). Since $\Delta W^{P\Pi} > 0$ throughout, the POVM-based engine always possesses an advantage over the PVM-based engine in terms of optimal work extraction. We further note that this advantage is independent of the cold-bath temperature. The figure also shows the auxiliary reset cost corresponding to the optimal POVM measurement, $[W_a^{V_0}]_m$ represented by the orange solid curve and given by Eq. (44), as a function of the cold-bath temperature T_c . For low values of T_c , the reset cost remains smaller than the advantage $\Delta W^{P\Pi}$ offered by the POVM-based engine. However, beyond a critical temperature T_c^{ad} , we obtain $\Delta W^{P\Pi} < [W_a^{V_0}]_m$. Consequently, for operating temperatures above T_c^{ad} , the net work output of the POVM-based Otto engine becomes smaller than that of the PVM-based engine. In this regime, the PVM-based engine becomes more advantageous once the auxiliary reset cost is taken into account.

2. Comparison for the non-adiabatic implementation

In Fig. 3, we compare the maximum work extractable from the PVM-based engine, \mathcal{W}_M^{Π} (red small dot-dashed), with the net work extractable from the POVM-based engine, for a fixed cold-bath inverse temperature $\beta_c = 1$. The quantity $\mathcal{W}_M^P - k_B T_c \ln 2$ (blue large dot-dashed) is presented as a lower bound on the net extractable work when the numerical optimization is performed over the system-auxiliary joint unitary V . We observe that over most of the parameter regime, the optimal work extracted from the PVM-based engine remains below this lower bound. In particular, in panel (b)

($\gamma > 2$), the lower bound remains greater than $\mathcal{W}_M^{\text{II}}$ throughout the entire range of P .

Further, when the net work itself is optimized over V , we obtain the quantity $[\mathcal{W}^P - \mathcal{W}_a]_M$, represented by the orange solid curve. This optimized net work remains significantly larger than the optimal work extracted from the PVM-based engine. Therefore, in the parameter regime considered here, the POVM-based engine provides a clear advantage over the PVM-based engine, even after accounting for the auxiliary reset cost.

VII. CONCLUSION

In this work, we investigated a measurement-driven quantum Otto engine in which the conventional hot thermalization stroke was replaced by quantum measurements. Motivated by the growing interest in measurement-based quantum thermal machines and their potential advantages in controllability, operational simplicity, and enhanced performance, we systematically analyzed the optimal work extraction achievable from such engines using a qubit working substance. The study was carried out in both the infinite-time (adiabatic) and finite-time (non-adiabatic) regimes, considering implementations based on both projective-valued measurements (PVMs) and generalized two-outcome positive operator-valued measurements (POVMs).

We show that measurement-based Otto engines retain the same efficiency as conventional two-bath Otto engines in the adiabatic limit, while nevertheless enabling enhanced work extraction. By optimizing over all allowed measurement protocols, we identified the maximum extractable work for both PVM- and two-outcome POVM-based engines and compared with that of conventional hot-bath-driven quantum Otto engines. For both adiabatic and non-adiabatic implementation we showed that measurement-based engines can yield higher work output than the conventional two-bath Otto cycles within suitable parameter regimes, particularly in experimentally relevant finite-temperature settings. Furthermore, we found that non-adiabatic implementations of the PV- as well as POVM-fueled engines can outperform than their adiabatic counterparts. We also identified the corresponding operational conditions, particularly in the case of PVM-fueled Otto engines. Moreover, measurement-fueled Otto cycles are able to operate as engines even in parameter regimes, where conventional Otto cycles fail to function as engines.

A central result of the present study was that, in the context of optimal work extraction, POVM-based engines can outperform their PVM-based counterparts in both the adiabatic limit and non-adiabatic regime. Even after incorporating the thermodynamic cost associated with resetting the auxiliary system required for POVM implementation, the resulting net work output can still exceed that achievable with PVM-based engines. In this regard, we identified parameter regimes particularly for the adiabatic limit.

Overall, our work provided a comprehensive comparative analysis of PV-, POVM-, and conventional two-bath quantum Otto engines, clarifying the regimes in which measurement-

driven engines exhibit enhanced thermodynamic performance. More broadly, the present study highlighted the potential of quantum measurements as useful resources for energy conversion at the quantum scale and may motivate further theoretical and experimental investigations toward the development of efficient finite-time quantum thermal devices and advanced measurement-assisted quantum heat engines.

ACKNOWLEDGMENTS

SM and DS acknowledge support from the Infosys scholarship for senior students at Harish-Chandra Research Institute.

APPENDICES

Appendix A: Brief discussion on conventional Otto engine

Let us discuss here the working of the traditional two bath Otto cycle. The first stroke of the cycle is the thermalization process with the cold bath. The system is connected to a cold bath of the inverse temperature β_c during this stroke. This stroke is isochoric because the Hamiltonian of the two-level system remains fixed during this stroke as $H^{(1)}$. Here, $H^{(1)} = (\hbar\omega_z\sigma_z)/2$, where σ_z represents the Pauli spin matrix along the z direction. This stroke yields the thermal state (Gibbs state), given by

$$\begin{aligned} \rho_0^C &= \frac{e^{-\beta_c H^{(1)}}}{\text{Tr}(e^{-\beta_c H^{(1)}})} \\ &= \frac{e^{-v_z}|0\rangle\langle 0| + e^{v_z}|1\rangle\langle 1|}{2 \cosh v_z}, \end{aligned} \quad (\text{A1})$$

where $v_z := (\hbar\beta_c\omega_z)/2$. The energy after the thermalizing stroke is evaluated as

$$E_0^C = \text{Tr}(H^{(1)}\rho_0^C) = -\frac{\hbar}{2}\omega_z \tanh v_z. \quad (\text{A2})$$

The second stroke consists of a unitary evolution of the Hamiltonian to $H^{(2)} = (\hbar\omega_x\sigma_x)/2$ starting from $H^{(1)}$, where σ_x represents the Pauli spin matrix along the x direction. The system is kept detached from the cold bath during this stroke. The change of energy due to this stroke is considered as work according to the entropy-based definition in quantum thermodynamics, because von-Neumann entropy remains constant in the course of unitary evolution. In the adiabatic limit, the state preserves the populations of the two-level system despite being diagonal on the eigen-basis of $H^{(2)}$, i.e., $\{|+\rangle, |-\rangle\}$. The final state and the corresponding energy after the completion of this stroke are given by, respectively,

$$\rho_1^C = p_1|+\rangle\langle +| + p_2|-\rangle\langle -|, \quad (\text{A3})$$

where $p_1 := e^{-v_x}/(2 \cosh v_x)$ and $p_2 := e^{v_x}/(2 \cosh v_x)$, and

$$E_1^C = \text{Tr}(\rho_1^C H^{(2)}) = -\frac{\hbar}{2}\omega_x \tanh v_x. \quad (\text{A4})$$

Here, we consider that the two unitary strokes are adiabatic. Therefore, each of the two unitary operations during these two unitary strokes effectively becomes Hadamard operation, which transforms between the eigenbasis of σ_z and σ_x . The work done during the first unitary stroke is given by

$$W_1^C = E_1^C - E_0^C = \frac{\hbar}{2} \tanh v_z (\omega_z - \omega_x). \quad (\text{A5})$$

During the third stroke, i.e., the second isochoric stroke, the system is attached to a hot bath of inverse temperature β_h , where $\beta_h < \beta_c$. This stroke yields the thermal state

$$\begin{aligned} \rho_2^C &= \frac{e^{-\beta_h H^{(2)}}}{\text{Tr}(e^{-\beta_h H^{(2)}})} \\ &= \frac{1}{2 \cosh v_x} (e^{-v_x} |+\rangle\langle +| + e^{v_x} |-\rangle\langle -|), \end{aligned}$$

where $v_x := (\hbar\beta_h\omega_x)/2$. The energy after the thermalizing stroke is evaluated as

$$E_2^C = \text{Tr}(H^{(2)}\rho_2) = -\frac{\hbar}{2}\omega_x \tanh v_x. \quad (\text{A6})$$

The change of energy due to this stroke is considered as heat because the Hamiltonian remains fixed during this stroke. The amount of transferred heat is given by

$$Q_h^C = E_2^C - E_1^C = \frac{\hbar}{2}\omega_x (\tanh v_z - \tanh v_x). \quad (\text{A7})$$

The fourth stroke is a unitary evolution which changes to the Hamiltonian of the system to $H^{(1)}$ from $H^{(2)}$. In the adiabatic limit, the populations of the two-level system in preserved despite being diagonal on the eigen-basis of $H^{(1)}$, i.e., $\{|+\rangle, |-\rangle\}$. The final state and the corresponding energy after the completion of this stroke are given by, respectively,

$$\rho_3^C = \frac{1}{2 \cosh v_x} (e^{-v_x} |0\rangle\langle 0| + e^{v_x} |1\rangle\langle 1|),$$

and $E_3^C = \text{Tr}(\rho_3^C H^{(1)}) = -\frac{\hbar}{2}\omega_z \tanh v_x$. The work done due to this stroke is evaluated as

$$W_2^C = E_3^C - E_2^C = \frac{\hbar}{2}(\omega_x - \omega_z) \tanh v_x. \quad (\text{A8})$$

From Eq. (8) and Eq. (A8), according to our adopted convention discussed in Subsec. II C, the total work W can be computed as

$$\begin{aligned} W^C &= -(W_1^C + W_2^C) \\ &= \frac{\hbar}{2}(\omega_x - \omega_z)(\tanh v_z - \tanh v_x). \end{aligned} \quad (\text{A9})$$

The amount of exchanged heat with the cold bath is given by

$$\begin{aligned} Q_c^C &= E_0^C - E_3^C \\ &= \frac{\hbar}{2}\omega_z (\tanh v_x - \tanh v_z) \end{aligned} \quad (\text{A10})$$

From Eq. (A9), Eq. (A7) and Eq. (A10), we obtain $Q_h^C + Q_c^C = W^C$, which verifies the consistency with the first law of thermodynamics.

The efficiency of the engine is given by

$$\eta^C = \frac{W^C}{Q_h^C} = 1 - \frac{\omega_z}{\omega_x}. \quad (\text{A11})$$

The requirement for the device to operate as an engine is that the work done is performed by the engine, i.e., $W^C < 0$ according to our convention. The physical requirement of $\eta^C \leq 1$ gives us the criterion, i.e., $\omega_z \leq \omega_x$. Now, $\omega_z = \omega_x$ is not physically acceptable for behaving as an engine, because it makes the net work $W^C = 0$ according to Eq. (A9). Therefore, the equality does not hold, and we obtain $\omega_z < \omega_x$ which also leads that $\eta^C < 1$.

When $\omega_z < \omega_x$ is satisfied, the required negativity of the RHS of Eq. (A9) gives us $(\tanh v_z - \tanh v_x) > 0$ which yields

$$\frac{\omega_z}{\omega_x} > \frac{\beta_h}{\beta_c}. \quad (\text{A12})$$

Eq. (A12) confirms that the Otto engine can not overcome the Carnot's efficiency, i.e., $1 - \frac{\beta_h}{\beta_c}$. It is a physically consistent result.

Appendix B: Conventional Otto engine in non-adiabatic regime

The behavior of the quantum Otto cycle, including the non-adiabatic regime, is discussed in [55]. The energies after the cold bath thermalization and the following first unitary stroke are given by

$$\mathcal{E}_0^C = -\frac{\hbar}{2}\omega_z \tau_z, \quad (\text{B1})$$

$$\text{and } \mathcal{E}_1^C = \frac{\hbar \tau_z}{2} \omega_x (1 - 2P), \quad (\text{B2})$$

respectively, where $P := |\langle +|U|0\rangle|^2$. Subtracting, the work $\mathcal{W}_1^C = \mathcal{E}_1^C - \mathcal{E}_0^C$ associated with the first unitary stroke is obtained

$$\mathcal{W}_1^C = \frac{\hbar \tau_z}{2} (\omega_x (1 - 2P) + \omega_z). \quad (\text{B3})$$

Similarly, the energies after the hot bath thermalization and the following second unitary stroke are given by

$$\mathcal{E}_2^C = -\frac{\omega_x \tau_x}{2}, \quad (\text{B4})$$

$$\text{and } \mathcal{E}_3^C = \frac{\hbar \tau_x}{2} \omega_z (1 - 2\tilde{P}), \quad (\text{B5})$$

respectively, where $\tilde{P} := |\langle 0|\tilde{U}|+\rangle|^2$. Subtracting, the work $\mathcal{W}_2^C = \mathcal{E}_3^C - \mathcal{E}_2^C$ associated with the second unitary stroke is obtained

$$\mathcal{W}_2^C = \frac{\hbar \tau_x}{2} (\omega_z (1 - 2\tilde{P}) + \omega_x), \quad (\text{B6})$$

Therefore, from Eq. (B3) and Eq. (B6), the total work $\mathcal{W}^C = -(\mathcal{W}_1^C + \mathcal{W}_2^C)$ is obtained

$$\mathcal{W}^C = \frac{\hbar}{2} [\tau_z(\omega_x(2P-1) - \omega_z) + \tau_x(\omega_z(2\tilde{P}-1) - \omega_x)] \quad (\text{B7})$$

The exchanged heat associated with the cold bath and hot bath thermalization strokes are given by

$$\mathcal{Q}_c^C = \mathcal{E}_0^C - \mathcal{E}_3^C = -\frac{\hbar\omega_z}{2} (\tau_z + \tau_x(1-2\tilde{P})) \quad (\text{B8})$$

$$\mathcal{Q}_h^C = \mathcal{E}_2^C - \mathcal{E}_1^C = -\frac{\hbar\omega_x}{2} (\tau_x + \tau_z(1-2P)) \quad (\text{B9})$$

From Eq. (B7), Eq. (B8), and Eq. (B9), it can be checked that $\mathcal{Q}_c^C + \mathcal{Q}_h^C = \mathcal{W}^C$ is satisfied, showing that the first law of thermodynamics is not violated.

Therefore, from Eq. (B7) and Eq. (B9), the efficiency $\eta_{ma}^C = \mathcal{W}^C/\mathcal{Q}_h^C = 1 + (\mathcal{Q}_c^C/\mathcal{Q}_h^C)$ of the engine can be evaluated

$$\eta_{ma}^C = 1 + \frac{\omega_z(\tau_z + \tau_x(1-2\tilde{P}))}{\omega_x(\tau_x + \tau_z(1-2P))} \quad (\text{B10})$$

Considering $\tilde{U} = U^\dagger$, we obtain $\tilde{P} = |\langle 0|U^\dagger|+\rangle|^2 = \langle 0|U^\dagger|+\rangle\langle 0|U^\dagger|+\rangle^* = \langle +|U|0\rangle^*\langle +|U|0\rangle = |\langle +|U|0\rangle|^2 = P$, with which Eq. (B7) and Eq. (B10) reduce to

$$\mathcal{W}^C = \frac{\hbar}{2} [\tau_z(\omega_x(2P-1) - \omega_z) + \tau_x(\omega_z(2P-1) - \omega_x)], \quad (\text{B11})$$

$$\text{and } \eta_{ma}^C = 1 + \frac{\omega_z(\tau_z + \tau_x(1-2P))}{\omega_x(\tau_x + \tau_z(1-2P))}, \quad (\text{B12})$$

respectively. \mathcal{W}^C is not necessarily positive for the entire range of P , i.e., $P \in [1/2, 1]$. The regimes where $\mathcal{W}_{2b} > 0$ holds for a particular setup, the Otto cycle operates as an engine.

Now, let us investigate when \mathcal{W}^C is maximum. Differentiating the both sides of Eq. (B11) w.r.t. P , we obtain $\frac{\partial \mathcal{W}^C}{\partial P} = \hbar(\tau_z\omega_x + \tau_x\omega_z)$, which is a strictly positive quantity for the entire domain of P , i.e., $P \in [1/2, 1]$. As $\frac{\partial \mathcal{W}^C}{\partial P} > 0$, the maximum value of \mathcal{W}^C is attained at $P = 1$, i.e., the adiabatic limit. Therefore, The efficiency at optimal work extraction is found $\eta_{ma}^C = 1 - (\omega_z/\omega_x)$.

Furthermore, when $\beta_h = 0$, the extracted work is given by

$$[\mathcal{W}^C]_{\beta_h=0} = \frac{\hbar}{2} [\tau_z(\omega_x(2P-1) - \omega_z)]. \quad (\text{B13})$$

Subtracting Eq. (B13) from Eq. (B11), we obtain

$$\mathcal{W}^C - [\mathcal{W}^C]_{\beta_h=0} = \tau_x(\omega_z(2P-1) - \omega_x). \quad (\text{B14})$$

Since $\omega_x > \omega_z$ and $2P-1 \in [0, 1]$ hold, $\omega_x > \omega_z(2P-1)$ also holds good, implying that the RHS of Eq. (B14) is negative, leading to $[\mathcal{W}^C]_{\beta_h=0} > \mathcal{W}^C$. Therefore, when the Otto cycle performs as an engine for a given set of β_h and P ,

then the extractable work \mathcal{W}^C can be increased by lowering β_h , and finally it becomes maximum when $\beta_h = 0$, i.e., the hot bath is taken to infinite temperature. In both the panels of Fig. 2, Eq. (B11) and Eq. (B13) are illustrated by the blue and orange-colored curves, respectively.

Appendix C: Derivation of Eq. (20)

Let us evaluate $\mathcal{E}_2^\Pi = \text{Tr}(H^{(2)}\rho_2^\Pi)$ for the PVM-based Otto cycle. Putting $\rho_2^\Pi = p_\psi|\psi\rangle\langle\psi| + p_{\psi^\perp}|\psi^\perp\rangle\langle\psi^\perp|$, we obtain

$$\mathcal{E}_2^\Pi = p_\psi\langle\psi|H^{(2)}|\psi\rangle + p_{\psi^\perp}\langle\psi^\perp|H^{(2)}|\psi^\perp\rangle. \quad (\text{C1})$$

The spectral decomposition of $H^{(1)}$ can be written as $H^{(1)} = \sum_{k=1}^2 E_k^{(1)}|\psi_k^{(1)}\rangle\langle\psi_k^{(1)}|$, where $k=1$ corresponds to $E_1^{(1)} = \frac{\omega_z}{2}$ and $|\psi_1^{(1)}\rangle = |0\rangle$, and $k=2$ corresponds to $E_2^{(1)} = -\frac{\omega_z}{2}$ and $|\psi_2^{(1)}\rangle = |1\rangle$. Similarly, the spectral decomposition of $H^{(2)}$ can be written as $H^{(2)} = \sum_{k=1}^2 E_k^{(2)}|\psi_k^{(2)}\rangle\langle\psi_k^{(2)}|$, where $k=1$ corresponds to $E_1^{(2)} = \frac{\omega_x}{2}$ and $|\psi_1^{(2)}\rangle = |+\rangle$, and $k=2$ corresponds to $E_2^{(2)} = -\frac{\omega_x}{2}$ and $|\psi_2^{(2)}\rangle = |-\rangle$. With the spectral decomposition of $H^{(2)}$, we obtain $\langle\psi|H^{(2)}|\psi\rangle = \sum_k E_k^{(2)}|\langle\psi|\psi_k^{(2)}\rangle|^2$ and $\langle\psi^\perp|H^{(2)}|\psi^\perp\rangle = \sum_k E_k^{(2)}|\langle\psi^\perp|\psi_k^{(2)}\rangle|^2$. Let us consider $B := |\langle\psi|\psi_1^{(2)}\rangle|^2$, and then we obtain $|\langle\psi^\perp|\psi_1^{(2)}\rangle|^2 = |\langle\psi|\psi_2^{(2)}\rangle|^2 = 1-B$ and $|\langle\psi^\perp|\psi_2^{(2)}\rangle|^2 = B$, which give $|\langle\psi|H^{(2)}|\psi\rangle| = \frac{\omega_x}{2}(2B-1)$ and $|\langle\psi^\perp|H^{(2)}|\psi^\perp\rangle| = \frac{\omega_x}{2}(1-2B)$. Now, with $p_{\psi^\perp} = 1-p_\psi$, Eq. (C1) becomes

$$\mathcal{E}_2^\Pi = \frac{\omega_x}{2}(2B-1)(2p_\psi-1). \quad (\text{C2})$$

Now, $p_\psi = \langle\psi|\rho_1|\psi\rangle$. With $\rho_1 = U\rho_0U^\dagger$ and $\rho_0 = \sum_j p_j|\psi_j^{(1)}\rangle\langle\psi_j^{(1)}|$, we obtain $p_\psi = \sum_j p_j|\langle\psi|U|\psi_j^{(1)}\rangle|^2$. Let, $A := |\langle\psi|U|\psi_1^{(1)}\rangle|^2$ and we obtain $|\langle\psi^\perp|U|\psi_1^{(1)}\rangle|^2 = 1-A$. Now, p_ψ can be rewritten as $2p_\psi-1 = p_1A+p_2(1-A)$. Putting p_1 and p_2 given in Sec. II B 1, we obtain $2p_\psi-1 = \tau_z(1-2A)$, which reduces Eq. (C2) to

$$\mathcal{E}_2^\Pi = -\frac{\omega_x\tau_z}{2}(2B-1)(2A-1),$$

which is Eq. (20). Hence, Eq. (20) is derived.

Appendix D: Derivation of Eq. (22)

Let us evaluate $\mathcal{E}_3^\Pi = \text{Tr}(H^{(1)}\rho_3)$ for the PVM-based Otto cycle. Plugging the spectral decomposition of $H^{(1)}$ discussed in Appendix C, and $\rho_3 = \tilde{U}\rho_2\tilde{U}^\dagger$, we obtain

$$\mathcal{E}_3^\Pi = \sum_{i,j,k} E_k^{(1)} p_j |\langle\psi_i|U|\psi_j^{(1)}\rangle|^2 Q_{ki}, \quad (\text{D1})$$

where $Q_{ki} := |\langle\psi_k^{(1)}|\tilde{U}|\psi_i\rangle|^2$. Let us denote $Q := |\langle\psi_1^{(1)}|\tilde{U}|\psi\rangle|^2$. Accordingly, we obtain $|\langle\psi_1^{(1)}|\tilde{U}|\psi^\perp\rangle|^2 =$

$|\langle \psi_2^{(1)} | \tilde{U} | \psi \rangle|^2 = 1 - Q$ and $|\langle \psi_2^{(1)} | \tilde{U} | \psi^\perp \rangle|^2 = Q$. Now, Eq. (D1) becomes

$$\begin{aligned} \mathcal{E}_3^\Pi = & h_\psi^{(1)} \sum_j (p_j |\langle \psi | U | \psi_j^{(1)} \rangle|^2) \\ & + h_{\psi^\perp}^{(1)} \sum_j (p_j |\langle \psi^\perp | U | \psi_j^{(1)} \rangle|^2), \end{aligned} \quad (\text{D2})$$

where $h_\psi^{(1)} := \sum_k E_k^{(1)} |\langle \psi_k^{(1)} | \tilde{U} | \psi \rangle|^2 = \omega_z(2Q - 1)/2$ and $h_{\psi^\perp}^{(1)} := \sum_k E_k^{(1)} |\langle \psi_k^{(1)} | \tilde{U} | \psi^\perp \rangle|^2 = \omega_z(1 - 2Q)/2$. Hence, Eq. (D2) reduces to

$$\mathcal{E}_3^\Pi = \frac{\omega_z}{2} (2Q - 1)(2p_\psi - 1), \quad (\text{D3})$$

with $p_\psi = \sum_j p_j |\langle \psi | U | \psi_j^{(1)} \rangle|^2$. In Appendix C, we have already derived $2p_\psi - 1 = \tau_z(1 - 2A)$, which reduces Eq. (D3) to

$$\mathcal{E}_3^\Pi = -\frac{\tau_z \omega_z}{2} (2Q - 1)(2A - 1),$$

which is Eq. (22). Hence, Eq. (22) is derived.

Appendix E: Analytical optimization of work extraction in the non-adiabatic PVM-based Otto engine

To find the optimal value of the work, given by Eq. (26), we analyze the extremum points as well as the boundary values. Putting $\theta = 0$, Eq. (26) gives

$$[\mathcal{W}^\Pi]_{\theta=0} = -2\omega_z \tau_z P(1 - P) \leq 0, \quad (\text{E1})$$

for $P \in [1/2, 1]$, where the equality holds for $P = 1$. The two boundary values $\theta = 0, \pi$ correspond to the same basis of measurement, $\{|+\rangle, |-\rangle\}$, leading to $\mathcal{W}^\Pi \leq 0$, concluding that the Otto cycle does not run as an engine at the two boundary values of θ .

Now, let us find the intermediate extremum point. From the discussion in Sec. IV B, we obtain

$$\mu = a \cos \theta_x + b \sin \theta_x \cos(\phi_x - \alpha), \quad (\text{E2})$$

where $a := 2P - 1$, $b := 2\sqrt{P(1 - P)}$. Now, partially differentiating μ w.r.t. ϕ and θ , respectively, we obtain,

$$\frac{\partial \mu}{\partial \phi_x} = -b \sin \theta_x \sin(\phi - \alpha), \quad (\text{E3})$$

$$\frac{\partial \mu}{\partial \theta_x} = -a \sin \theta_x + b \cos \theta_x \cos(\phi - \alpha). \quad (\text{E4})$$

Partially differentiating W given by Eq. (26) w.r.t. ϕ and θ , respectively, we obtain

$$\frac{\partial \mathcal{W}^\Pi}{\partial \phi_x} = \frac{\hbar \tau_z}{2} (2\omega_z \mu - \omega_x \cos \theta_x) \frac{\partial \mu}{\partial \phi_x}, \quad (\text{E5})$$

$$\frac{\partial \mathcal{W}^\Pi}{\partial \theta_x} = \frac{\hbar \tau_z}{2} \left((2\omega_z \mu - \omega_x \cos \theta_x) \frac{\partial \mu}{\partial \theta_x} + \omega_x \mu \sin \theta_x \right), \quad (\text{E6})$$

where $\frac{\partial \mu}{\partial \phi_x}$ and $\frac{\partial \mu}{\partial \theta_x}$ are to be plugged from Eq. (E3) and Eq. (E4), respectively.

Equating $\frac{\partial \mathcal{W}^\Pi}{\partial \phi}$ given by Eq. (E5) with zero, we obtain the two following cases - **case 1**: $\omega_x \cos \theta_x = 2\omega_z \mu$ and **case 2**: $\frac{\partial \mu}{\partial \phi_x} = 0$.

Case-1: If case-1 holds, then Eq. (E6) reduces to $\sin \theta_x = 0$, leading to $\theta_x \in \{0, \pi\}$, which in turn corresponds to the boundary cases of θ_x in the domain of θ_x , i.e., $\theta_x \in [0, \pi]$. We have already discussed this scenario; accordingly, this case can not lead to the optimal work extraction.

Case 2: Case 2 gives $\sin \theta_x \sin(\phi_x - \alpha) = 0$, which yields two subclasses - **2(a)**: $\sin \theta_x = 0$, which essentially leads to Case 1. **2(b)**: $\sin(\phi_x - \alpha) = 0$, which leads to $\phi - \alpha = 0, \pm\pi$.

Therefore, case 2 gives us a valid condition for optimality, as the following: $\phi_x - \alpha = 0, \pm\pi$, which gives $\cos(\phi_x - \alpha) = s \in \{1, -1\}$.

With this optimality condition, Eq. (E2), Eq. (E4) and Eq. (26) reduce to, respectively,

$$\mu = a \cos \theta_x + sb \sin \theta_x, \quad (\text{E7})$$

$$\frac{\partial \mu}{\partial \theta_x} = -a \sin \theta_x + sb \cos \theta_x, \quad (\text{E8})$$

$$\begin{aligned} \text{and } \mathcal{W}^\Pi = & -\frac{\hbar \tau_z}{4} \left[-2a\omega_x + \omega_z + \omega_x a + (a\omega_x \cos x \right. \\ & \left. - \omega_z(a^2 - b^2)) + sb(\omega_x - 2a\omega_z) \sin x \right], \end{aligned} \quad (\text{E9})$$

where $s \in \{1, -1\}$. As Eq. (E7) and Eq. (E8) hold, Eq. (E6) reduces to $\frac{\partial \mathcal{W}^\Pi}{\partial \theta_x} = \hbar \tau_z (-A \sin x + sB \cos x)/2$, where $A := \omega_z(b^2 - a^2) + a\omega_x$, $B := b(\omega_x - 2a\omega_z)$, and $x := 2\theta$. Equating $\frac{\partial \mathcal{W}^\Pi}{\partial \theta_x}$ with zero, we obtain

$$A \sin x = sB \cos x. \quad (\text{E10})$$

As the boundary cases of θ does not lead to optimality, we get $\cos x \neq 0$, therefore, Eq. (E10) gives

$$\tan x = \frac{sB}{A}. \quad (\text{E11})$$

Squaring both sides of Eq. (E10) and using the identity $\sin^2 x + \cos^2 x = 1$, we obtain

$$\cos x = \frac{s'A}{\sqrt{A^2 + B^2}} \quad (\text{E12})$$

$$\begin{aligned} \text{and } \sin x = & \frac{sB}{A} \cos x \\ = & \frac{ss'B}{\sqrt{A^2 + B^2}}, \end{aligned} \quad (\text{E13})$$

where s' corresponds to the two solutions of the quadratic equation $s' \in \{1, -1\}$. Plugging the RHSs of Eq. (E13) and

Eq. (E12) into Eq. (E9), we obtain

$$\begin{aligned}\mathcal{W}^\Pi &= \frac{\hbar\tau_z}{4} (a\omega_x - \omega_z - s' \sqrt{A^2 + B^2}) \\ &= \frac{\hbar\tau_z}{4} \left((2P - 1)\omega_x - \omega_z \right. \\ &\quad \left. - s' \sqrt{(\omega_x - \omega_z)^2 + 4\omega_x\omega_z(1 - P)} \right),\end{aligned}\quad (\text{E14})$$

with $P \in [\frac{1}{2}, 1]$ and $s' \in \{1, -1\}$. For $s' = 1$, the RHS of Eq. (E14) becomes positive, which implies that the Otto cycle does not act as an engine. So, we focus on $s' = -1$ to investigate whether the Otto cycle performs as an engine. Hence, the optimal extractable work from the PVM-based Otto cycle is given by

$$\mathcal{W}_M^\Pi = \frac{\hbar\tau_z}{4} \left(\sqrt{(\omega_x - \omega_z)^2 + 4\omega_x\omega_z(1 - P)} - \omega_z + \omega_x(2P - 1) \right),$$

which is Eq. (27), depicted in the insets of Fig. 2. Thus, we have obtained the optimal work for a given P value.

Let us compute the Hessian matrix. Partially differentiating the both sides of Eq. (E5) w.r.t. ϕ_x , we obtain

$$\frac{\partial^2 \mathcal{W}^\Pi}{\partial \phi_x^2} = \frac{\hbar\tau_z}{2} \left((2\omega_z\mu - \omega_x \cos \theta_x) \frac{\partial^2 \mu}{\partial \phi_x^2} + 2\omega_z \left(\frac{\partial \mu}{\partial \phi_x} \right)^2 \right).\quad (\text{E15})$$

Now, $\frac{\partial \mu}{\partial \phi_x} = 0$ at the optimality condition. Also, partially differentiating both sides of Eq. (E3) w.r.t. ϕ_x , we obtain $\frac{\partial^2 \mu}{\partial \phi_x^2} = -b \sin \theta_x \cos(\phi_x - \alpha)$, which reduces to $-sb \sin \theta_x$ at the optimality condition. So, the RHS of Eq. (E15) becomes $-\tau_z sb(\omega_z\mu \sin \theta_x - (\omega_x/4) \sin x)$, with $2\theta_x = x$. Now, we plug $\sin x$ from Eq. (E13), simplify with $s^2 = 1$, and obtain

$$\frac{\partial^2 \mathcal{W}^\Pi}{\partial \phi_x^2} = -\hbar\tau_z b \left(s\omega_z\mu \sin \theta_x - \frac{\omega_x}{4} \frac{s'B}{\sqrt{A^2 + B^2}} \right).\quad (\text{E16})$$

We also perform partial differentiation of the both sides of Eq. (E6) w.r.t. θ , then plug $\cos x$ and $\sin x$ from Eq. (E12) and Eq. (E13) respectively, and finally obtain

$$\frac{\partial^2 \mathcal{W}^\Pi}{\partial \theta^2} = \hbar s' \tau_z \sqrt{A^2 + B^2}\quad (\text{E17})$$

Now, let us compute the off-diagonal elements of the Hessian matrix. Partially differentiating both sides of Eq. (E5) w.r.t. θ , we obtain

$$\begin{aligned}\frac{\partial^2 \mathcal{W}^\Pi}{\partial \theta_x \partial \phi_x} &= \frac{\hbar\tau_z}{2} \left[(2\omega_z\mu - \omega_x \cos \theta_x) \frac{\partial^2 \mu}{\partial \theta_x \partial \phi_x} \right. \\ &\quad \left. + (2\omega_z \frac{\partial \mu}{\partial \theta_x} + \omega_x \sin \theta_x) \frac{\partial \mu}{\partial \phi_x} \right].\end{aligned}\quad (\text{E18})$$

Partially differentiating both sides of Eq. (E3) w.r.t. θ , we get $\frac{\partial^2 \mu}{\partial \theta_x \partial \phi_x} = -b \cos \theta_x \sin(\phi_x - \alpha)$, which vanishes at the optimality condition. As $\frac{\partial^2 \mu}{\partial \theta_x \partial \phi_x} = 0$ and $\frac{\partial \mu}{\partial \phi_x} = 0$ hold at

the optimality condition, the RHS of Eq. (E18) becomes zero. As, W is a regular function, the two off-diagonal elements are the same due to the property of the partial differentiation. Eq. (E16) and Eq. (E17), with $s' = -1$, gives the Hessian matrix:

$$\begin{aligned}&\begin{pmatrix} \frac{\partial^2 \mathcal{W}^\Pi}{\partial \phi_x^2} & \frac{\partial^2 \mathcal{W}^\Pi}{\partial \theta_x \partial \phi_x} \\ \frac{\partial^2 \mathcal{W}^\Pi}{\partial \phi_x \partial \theta_x} & \frac{\partial^2 \mathcal{W}^\Pi}{\partial \theta_x^2} \end{pmatrix}_{\text{optimal}} \\ &= \begin{pmatrix} -\hbar\tau_z b \left(s\omega_z\mu \sin \theta_x + \frac{\omega_x}{4} \frac{B}{\sqrt{A^2 + B^2}} \right) & 0 \\ 0 & -\hbar\tau_z \sqrt{A^2 + B^2} \end{pmatrix},\end{aligned}$$

of which the two diagonal elements are the two eigenvalues because the off-diagonal elements are zero. Since $\theta \in [0, \pi]$, $\sin \theta_x > 0$, therefore $-\hbar\tau_z b \left(s\omega_z\mu \sin \theta_x + \frac{\omega_x}{4} \frac{B}{\sqrt{A^2 + B^2}} \right) < 0$ when $s = 1$. Also, the other eigenvalue $-\hbar\tau_z \sqrt{A^2 + B^2} < 0$. Thus $s = 1$ and $s' = -1$ together maximize \mathcal{W}^Π . With $s = 1$ and $s' = -1$, the optimal θ can be obtained from either of Eq. (E11), Eq. (E12), Eq. (E13).

Now, we analyze the value of P , for which \mathcal{W}_M^Π is maximum. At first, we analyze the two boundary values of P . At $P = 1/2$ and $P = 1$, we obtain, respectively,

$$[\mathcal{W}_M^\Pi]_{P=1/2} = \frac{\hbar\tau_z}{4} (\sqrt{\omega_x^2 + \omega_z^2} - \omega_z) \quad \text{and} \quad (\text{E19})$$

$$[\mathcal{W}_M^\Pi]_{P=1} = \frac{\hbar\tau_z}{2} (\omega_x - \omega_z).\quad (\text{E20})$$

Since, $\omega_x^2 + \omega_z^2 > \omega_z^2$, therefore, $\sqrt{\omega_x^2 + \omega_z^2} > \omega_z$, which renders the RHS of Eq. (E19) positive. Similarly, since $\omega_z < \omega_x$, the RHS of Eq. (E20) is also positive. Now, we analyze whether any intermediate extremum point exists. We evaluate

$$\frac{\partial \mathcal{W}^\Pi}{\partial P} = \frac{\hbar\tau_z \omega_z}{2} \left(1 - \frac{\omega_z}{\sqrt{(\omega_x - \omega_z)^2 + 4\omega_z\omega_x(1 - P)}} \right)$$

Equating $\frac{\partial \mathcal{W}^\Pi}{\partial P} = 0$, we obtain that there is one extremum point at the particular value of P , i.e., $P_0 = \frac{1}{2} + \frac{\gamma}{4}$, where $\gamma := \omega_x/\omega_z$ is the compression ratio. We also find that

$$\left[\frac{\partial^2 \mathcal{W}^\Pi}{\partial P^2} \right]_{P=P_0} = -\frac{\hbar\tau_z (\omega_x \omega_z)^2}{2((\omega_x - \omega_z)^2 + 4\omega_z\omega_x(1 - P))^{3/2}} < 0,$$

which ensures that this point gives the maximum of \mathcal{W}^Π . Since the domain of P is given by $P \in [1/2, 1]$, this intermediate extremum value exists when $\gamma < 2$.

When $\gamma < 2$: There is only one intermediate extremum point, which is found to be a maximum. Hence, this point is the global maxima.

When $\gamma \geq 2$: For $\gamma = 2$, we find that $P_0 = 1$, hence coincides with one of the boundary points. For $\gamma > 2$, we find that $P_0 > 1$, which lies outside the domain of P , implying that the intermediate extremum point does not exist in that regime, and the maximum of W is at any of the boundary values of P . With some algebraic steps, we obtain that $[\mathcal{W}_M^\Pi]_{P=1} > [\mathcal{W}_M^\Pi]_{P=1/2}$ for all $\gamma \geq 2$. So, the global maxima lies at $P = 1$, which is the adiabatic limit.

Moreover, we see that $\mathcal{W}^{\text{II}} > 0$ holds for the two boundary points, with no intermediate extremum point for $\gamma \geq 2$, and for $\gamma < 2$ there is only one extremum point which is found to be a maximum, so we can conclude that $\mathcal{W}^{\text{II}} > 0$ holds good for all values of $P \in [1/2, 1]$, implying that the PVM-based Otto cycle runs as an engine for the entire domain of P .

Appendix F: Efficiency at the optimal work extraction in the non-adiabatic PVM-base Otto engine

For any given value of the non-adiabaticity parameter P , the optimally extractable work \mathcal{W}^{II} is given by Eq. (27). The heat injected by the measurement stroke is evaluated

$$\mathcal{Q}_h^{\text{II}} = \frac{\omega_x v_z (a(D - (4a^2 - 3)\omega_z) + 8(P - 1)P\omega_x + \omega_x)}{4D}, \quad (\text{F1})$$

with $a := 2P - 1$ and $D := \sqrt{(\omega_x - \omega_z)^2 + 4\omega_x\omega_z(1 - P)}$. From Eq. (27) and Eq. (F1), we obtain the efficiency $\eta_{\text{na}}^{\text{II}} = \mathcal{W}_M^{\text{II}}/\mathcal{Q}_h^{\text{II}}$ for any given value of P ,

$$\eta_{\text{na}}^{\text{II}} = \frac{D(D + a\omega_x - \omega_z)}{\omega_x(a(D - (4a^2 - 3)\omega_z) + 8(P - 1)P\omega_x + \omega_x)}. \quad (\text{F2})$$

Appendix G: Detailed derivation of Eq. (33)

Let us explicitly evaluate $E_2^{\mathcal{P}}$ in the case of the POVM-based adiabatic Otto engine. Using Eq. (32), we have

$$\begin{aligned} E_2^{\mathcal{P}} &= \text{Tr} \left((H^{(2)} \otimes I) \rho'_{sa} \right) \\ &= \text{Tr} \left((H^{(2)} \otimes I) \sum_{i=1}^2 (I \otimes \Pi_i) (V \rho_{sa} V^\dagger) (I \otimes \Pi_i) \right) \\ &= \sum_{i=1}^2 \text{Tr} \left((H^{(2)} \otimes \Pi_i) (V \rho_{sa} V^\dagger) (I \otimes \Pi_i) \right) \\ &= \sum_{i=1}^2 \text{Tr} \left((H^{(2)} \otimes \Pi_i) (V \rho_{sa} V^\dagger) \right) \\ &= \text{Tr} \left(H^{(2)} \otimes \left[\sum_{i=1}^2 \Pi_i \right] (V \rho_{sa} V^\dagger) \right) \\ &= \text{Tr} \left((H^{(2)} \otimes I) (V \rho_{sa} V^\dagger) \right) \end{aligned}$$

Here we have used $(A \otimes B)(C \otimes D) = (AC) \otimes (BD)$ in the second, $\Pi_i^2 = \Pi_i$ in the third, and $\sum_{i=1}^2 \Pi_i = I$ in the last lines. Thus, Eq. (33) is derived.

Appendix H: Construction of the swap operator

Expressing the the identity operator as $I = |+\rangle\langle+| + |-\rangle\langle-|$ and $H^{(2)}$ as given by Eq. (2), we can write $H^{(2)} \otimes I$ as

$$\begin{aligned} H^{(2)} \otimes I &= \frac{\hbar}{2} \omega_x (|++\rangle\langle++| + |+-\rangle\langle+-| \\ &\quad - |-+\rangle\langle-+| - |--\rangle\langle--|), \end{aligned}$$

which clearly shows that the eigenstates $\{|++\rangle, |+-\rangle\}$ are associated with the two degenerate higher energy eigenvalues $\hbar\omega_x/2$ and $\{|-+\rangle, |--\rangle\}$ are associated with the two degenerate lower energy eigenvalues $-\hbar\omega_x/2$.

Furthermore, with the help of Eq. (A3) and plugging $\rho_a = |+\rangle\langle+|$, the bipartite state ρ_{sa} is obtained as $(e^{-v_z}|+\rangle\langle+| + e^{v_z}|-\rangle\langle-|)/(2 \cosh v_z)$, showing that $\text{supp}(\rho_{sa}) = \{|+\rangle, |-\rangle\}$, being associated with only two non-zero eigenvalues.

Appendix I: Considering mixed auxiliary states

Let us consider that the auxiliary system is initially in an arbitrary mixed state $\rho_a = q|\tilde{\psi}\rangle\langle\tilde{\psi}| + (1 - q)|\tilde{\psi}^\perp\rangle\langle\tilde{\psi}^\perp|$, where q is the the mixing parameter which satisfies $0 \leq q \leq 1$. Here, the eigenvalues of ρ_a are q and $1 - q$. Therefore, the four eigenvalues of $\rho_1 \otimes \rho_a$ are $qe^{-v_z}/(2 \cosh v_z)$, $(1 - q)e^{-v_z}/(2 \cosh v_z)$, $qe^{v_z}/(2 \cosh v_z)$, and $(1 - q)e^{v_z}/(2 \cosh v_z)$. Without the loss of generality, we can consider $q > 1 - q$. Furthermore, we restrict ourselves to the non-inverted population regime (excluding the effective negative temperature scenario), which implies the ordering $(1 - q)e^{v_z} > qe^{-v_z}$. Therefore, the eigenvalues are sorted as follows:

$$\frac{qe^{v_z}}{2 \cosh v_z} > \frac{(1 - q)e^{v_z}}{2 \cosh v_z} > \frac{qe^{-v_z}}{2 \cosh v_z} > \frac{(1 - q)e^{-v_z}}{2 \cosh v_z}.$$

Here, we obtain the maximum value of E_2 as the following:

$$\begin{aligned} (E_2^{\mathcal{P}})_M &= \left(\frac{\hbar}{2}\omega_x\right) \frac{qe^{v_z}}{2 \cosh v_z} + \left(\frac{\hbar}{2}\omega_x\right) \frac{(1 - q)e^{v_z}}{2 \cosh v_z} \\ &\quad + \left(-\frac{\hbar}{2}\omega_x\right) \frac{qe^{-v_z}}{2 \cosh v_z} + \left(-\frac{\hbar}{2}\omega_x\right) \frac{(1 - q)e^{-v_z}}{2 \cosh v_z} \\ &= \frac{\hbar}{2} \omega_x \tanh v_z. \end{aligned} \quad (\text{I1})$$

Thus we obtain the maximum value of W as

$$W_M^{\mathcal{P}} = \frac{\hbar}{2} (\omega_x - \omega_z) \tanh(v_z), \quad (\text{I2})$$

which is identical with the RHS of Eq. (14), i.e., the maximum extractable work from the PVM-based Otto engine. We conclude that taking the initial state of the auxiliary system as an arbitrary mixed state does not give any advantage over the PVM-based Otto engine.

- [1] J. Gemmer, M. Michel, and G. Mahler, *Quantum Thermodynamics: Emergence of Thermodynamic Behavior Within Composite Quantum Systems* (Springer Berlin Heidelberg, 2009).
- [2] S. Vinjanampathy and J. Anders, Quantum thermodynamics, *Contemporary Physics* **57**, 545 (2016).
- [3] *Thermodynamics in the Quantum Regime: Fundamental Aspects and New Directions* (Springer International Publishing, 2018).
- [4] S. Deffner and S. Campbell, *Quantum Thermodynamics*, 2053-2571 (Morgan & Claypool Publishers, 2019).
- [5] R. Alicki, The quantum open system as a model of the heat engine, *Journal of Physics A* **12** (1979).
- [6] R. Kosloff, A quantum mechanical open system as a model of a heat engine, *The Journal of Chemical Physics* **80**, 1625 (1984).
- [7] H. T. Quan, Y.-x. Liu, C. P. Sun, and F. Nori, Quantum thermodynamic cycles and quantum heat engines, *Phys. Rev. E* **76**, 031105 (2007).
- [8] A. E. Allahverdyan, R. S. Johal, and G. Mahler, Work extremum principle: Structure and function of quantum heat engines, *Phys. Rev. E* **77**, 041118 (2008).
- [9] M. O. Scully, K. R. Chapin, K. E. Dorfman, M. B. Kim, and A. Svidzinsky, Quantum heat engine power can be increased by noise-induced coherence, *Proceedings of the National Academy of Sciences* **108**, 15097 (2011).
- [10] O. Fialko and D. W. Hallwood, Isolated quantum heat engine, *Phys. Rev. Lett.* **108**, 085303 (2012).
- [11] R. Kosloff and A. Levy, Quantum heat engines and refrigerators: Continuous devices, *Annu. Rev. of Phys. Chem.* **65**, 365 (2014).
- [12] W. Niedenzu, D. Gelbwaser-Klimovsky, A. G. Kofman, and G. Kurizki, On the operation of machines powered by quantum non-thermal baths, *New Journal of Physics* **18**, 083012 (2016).
- [13] R. Uzdin, Coherence-induced reversibility and collective operation of quantum heat machines via coherence recycling, *Phys. Rev. Appl.* **6**, 024004 (2016).
- [14] A. Friedenberger and E. Lutz, When is a quantum heat engine quantum?, *Europhysics Letters* **120**, 10002 (2017).
- [15] W. Niedenzu, V. Mukherjee, A. Ghosh, A. G. Kofman, and G. Kurizki, Quantum engine efficiency bound beyond the second law of thermodynamics, *Nature Communications* **9**, 165 (2018).
- [16] L. M. Cangemi, C. Bhadra, and A. Levy, Quantum engines and refrigerators, *Physics Reports* **1087**, 1 (2024), quantum engines and refrigerators.
- [17] J. P. Palao, R. Kosloff, and J. M. Gordon, Quantum thermodynamic cooling cycle, *Phys. Rev. E* **64**, 056130 (2001).
- [18] Y. Rezek, P. Salamon, K. H. Hoffmann, and R. Kosloff, The quantum refrigerator: The quest for absolute zero, *Europhysics Letters* **85**, 30008 (2009).
- [19] T. Feldmann and R. Kosloff, Optimal performance of quantum refrigerators, *arXiv:0906.0986* (2009).
- [20] N. Linden, S. Popescu, and P. Skrzypczyk, How small can thermal machines be? the smallest possible refrigerator, *Phys. Rev. Lett.* **105**, 130401 (2010).
- [21] K. Joulain, J. Drevillon, Y. Ezzahri, and J. Ordóñez-Miranda, Quantum thermal transistor, *Phys. Rev. Lett.* **116**, 200601 (2016).
- [22] A. Riera-Campenya, M. Mehboudi, M. Pons, and A. Sanpera, Dynamically induced heat rectification in quantum systems, *Phys. Rev. E* **99**, 032126 (2019).
- [23] A. Mandarino, K. Joulain, M. D. Gómez, and B. Bellomo, Thermal transistor effect in quantum systems, *Phys. Rev. Appl.* **16**, 034026 (2021).
- [24] M. Majland, K. S. Christensen, and N. T. Zinner, Quantum thermal transistor in superconducting circuits, *Phys. Rev. B* **101**, 184510 (2020).
- [25] R. Ghosh, A. Ghoshal, and U. Sen, Quantum thermal transistors: Operation characteristics in steady state versus transient regimes, *Phys. Rev. A* **103**, 052613 (2021).
- [26] D. Bhargava, P. Chaki, A. Bhattacharyya, and U. Sen, Quantum transistors for heat flux in and out of working substance parts: harmonic vs transmon and kerr environs, *arXiv:2501.11629* (2025).
- [27] D. Tiwari, S. Bhattacharya, and S. Banerjee, Quantum thermal analogs of electric circuits: A universal approach, *Phys. Rev. Lett.* **135**, 020404 (2025).
- [28] A. Maity, P. Chaki, A. Ghoshal, and U. Sen, Quantum heat transformers, *New Journal of Physics* **28**, 014501 (2025).
- [29] R. Alicki and M. Fannes, Entanglement boost for extractable work from ensembles of quantum batteries, *Phys. Rev. E* **87**, 042123 (2013).
- [30] S. Bhattacharjee and A. Dutta, Quantum thermal machines and batteries, *The European Physical Journal B* **94**, 239 (2021).
- [31] F. Campaioli, S. Gherardini, J. Q. Quach, M. Polini, and G. M. Andolina, Colloquium: Quantum batteries, *Rev. Mod. Phys.* **96**, 031001 (2024).
- [32] C. M. Bender, D. C. Brody, and B. K. Meister, Entropy and temperature of a quantum carnot engine, *Proceedings of the Royal Society A: Mathematical, Physical and Engineering Sciences* **458**, 1519 (2002).
- [33] D. Gelbwaser-Klimovsky, R. Alicki, and G. Kurizki, Minimal universal quantum heat machine, *Phys. Rev. E* **87**, 012140 (2013).
- [34] H. T. Quan, Y.-x. Liu, C. P. Sun, and F. Nori, Quantum thermodynamic cycles and quantum heat engines, *Phys. Rev. E* **76**, 031105 (2007).
- [35] P. Abiuso and M. Perarnau-Llobet, Optimal cycles for low-dissipation heat engines, *Phys. Rev. Lett.* **124**, 110606 (2020).
- [36] M. J. Henrich, F. Rempp, and G. Mahler, Quantum thermodynamic otto machines: A spin-system approach, *EPJ ST* **151**, 157 (2007).
- [37] O. Abah, J. Roßnagel, G. Jacob, S. Deffner, F. Schmidt-Kaler, K. Singer, and E. Lutz, Single-ion heat engine at maximum power, *Phys. Rev. Lett.* **109**, 203006 (2012).
- [38] R. Uzdin and R. Kosloff, Universal features in the efficiency at maximal work of hot quantum otto engines, *EPL* **108** (2014).
- [39] B. Leggio and M. Antezza, Otto engine beyond its standard quantum limit, *Phys. Rev. E* **93**, 022122 (2016).
- [40] R. Kosloff and Y. Rezek, The quantum harmonic otto cycle, *Entropy* **19** (2017).
- [41] V. Mehta and R. S. Johal, Quantum otto engine with exchange coupling in the presence of level degeneracy, *Phys. Rev. E* **96**, 032110 (2017).
- [42] G. A. Barrios, F. Albarrán-Arriagada, F. A. Cárdenas-López, G. Romero, and J. C. Retamal, Role of quantum correlations in light-matter quantum heat engines, *Phys. Rev. A* **96**, 052119 (2017).
- [43] N. F. Del Grosso, F. C. Lombardo, F. D. Mazzitelli, and P. I. Villar, Quantum otto cycle in a superconducting cavity in the nonadiabatic regime, *Phys. Rev. A* **105**, 022202 (2022).
- [44] R. Kosloff, A quantum mechanical open system as a model of a heat engine, *J. Chem. Phys.* **80**, 1625 (1984).

- [45] E. Geva and R. Kosloff, On the classical limit of quantum thermodynamics in finite time, *J.Chem.Phys.* **97**, 4398 (1992).
- [46] R. Geva, E. and Kosloff, Three-level quantum amplifier as a heat engine: A study in finite-time thermodynamics, *Phys. Rev. E* **49**, 3903 (1994).
- [47] H. B. Mehta and O. Bharti, Performance analysis of an irreversible otto cycle using finite time thermodynamics, in *Proceedings of the World Congress on Engineering*, Vol. 2 (WCE London, UK, 2009) p. 1.
- [48] F. Wu, J. He, Y. Ma, and J. Wang, Efficiency at maximum power of a quantum otto cycle within finite-time or irreversible thermodynamics, *Phys. Rev. E* **90**, 062134 (2014).
- [49] A. Alecce, F. Galve, N. L. Gullo, L. Dell'Anna, F. Plastina, and R. Zambrini, Quantum otto cycle with inner friction: finite-time and disorder effects, *New.J.Phys* **17**, 075007 (2015).
- [50] J. Chen, C. Sun, and H. Dong, Boosting the performance of quantum otto heat engines, *Phys. Rev. E* **100**, 032144 (2019).
- [51] O. Abah and M. Paternostro, Shortcut-to-adiabaticity otto engine: A twist to finite-time thermodynamics, *Phys. Rev. E* **99**, 022110 (2019).
- [52] M. Kloc, P. Cejnar, and G. Schaller, Collective performance of a finite-time quantum otto cycle, *Phys. Rev. E* **100**, 042126 (2019).
- [53] J. Wang, J. He, and Y. Ma, Finite-time performance of a quantum heat engine with a squeezed thermal bath, *Phys. Rev. E* **100**, 052126 (2019).
- [54] S. Lee, J. Ha, M. and Park, and H. Jeong, Finite-time quantum otto engine: Surpassing the quasistatic efficiency due to friction, *Phys. Rev. E* **101**, 022127 (2020).
- [55] A. Solfanelli, M. Falsetti, and M. Campisi, Nonadiabatic single-qubit quantum otto engine, *Phys. Rev. B* **101**, 054513 (2020).
- [56] A. Das and V. Mukherjee, Quantum-enhanced finite-time otto cycle, *Phys.Rev.R* **2**, 033083 (2020).
- [57] S. Saryal and B. Agarwalla, Bounds on fluctuations for finite-time quantum otto cycle, *Phys. Rev. E* **103**, L060103 (2021).
- [58] Y. Shirai, K. Hashimoto, R. Tezuka, C. Uchiyama, and N. Hatano, Non-markovian effect on quantum otto engine: Role of system-reservoir interaction, *Phys.Rev.R* **3**, 023078 (2021).
- [59] D. Saha, A. Ghoshal, and U. Sen, Temperature- and interaction-tweaked efficiency boost of finite-time robust quantum otto engines, *arXiv:2309.11483* (2023).
- [60] H. T. Quan, Y. D. Wang, Y.-x. Liu, C. P. Sun, and F. Nori, Maxwell's demon assisted thermodynamic cycle in superconducting quantum circuits, *Phys. Rev. Lett.* **97**, 180402 (2006).
- [61] T. Uusnäkki, T. Mörstedt, W. Teixeira, M. Rasola, and M. Möttönen, Experimental realization of a quantum heat engine based on dissipation-engineered superconducting circuits, *arXiv:2502.20143* (2025).
- [62] G. Barontini and M. Paternostro, Ultra-cold single-atom quantum heat engines, *New Journal of Physics* **21**, 063019 (2019).
- [63] J. P. S. Peterson, T. B. Batalhão, M. Herrera, A. M. Souza, R. S. Sarthour, I. S. Oliveira, and R. M. Serra, Experimental characterization of a spin quantum heat engine, *Phys. Rev. Lett.* **123**, 240601 (2019).
- [64] M. H. M. Passos, A. C. Santos, M. S. Sarandy, and J. A. O. Huguenin, Optical simulation of a quantum thermal machine, *Phys. Rev. A* **100**, 022113 (2019).
- [65] J. Sheng, C. Yang, and H. Wu, Realization of a coupled-mode heat engine with cavity-mediated nanoresonators, *arXiv:2110.13022* (2021).
- [66] H.-G. Xu, J. Jin, N. G. de Almeida, and G. D. de Moraes Neto, Exploring the role of criticality in the quantum otto cycle fueled by the anisotropic quantum rabi-stark model, *arXiv:2407.09027* (2024).
- [67] K. Shende, M. Kandpal, Arvind, and K. Dorai, Experimental investigation of a quantum otto heat engine with shortcuts to adiabaticity implemented using counter-adiabatic driving, *arXiv:2412.20194* (2024).
- [68] T. Uusnäkki, M. Rasola, V. Vadimov, P. Singh, A. Darwish, and M. Möttönen, Autonomous quantum heat engine, *arXiv:2603.15355* (2026).
- [69] M. Hayashi and H. Tajima, Measurement-based formulation of quantum heat engines, *Phys. Rev. A* **95**, 032132 (2017).
- [70] J. Yi, P. Talkner, and Y. W. Kim, Single-temperature quantum engine without feedback control, *Phys. Rev. E* **96**, 022108 (2017).
- [71] A. Das and S. Ghosh, Measurement based quantum heat engine with coupled working medium, *Entropy* **21** (2019).
- [72] S. Chand and A. Biswas, Critical-point behavior of a measurement-based quantum heat engine, *Phys. Rev. E* **98**, 052147 (2018).
- [73] M. F. Anka, T. R. de Oliveira, and D. Jonathan, Measurement-based quantum heat engine in a multilevel system, *Phys. Rev. E* **104**, 054128 (2021).
- [74] Z. Lin, S. Su, J. Chen, J. Chen, and J. F. G. Santos, Suppressing coherence effects in quantum-measurement-based engines, *Phys. Rev. A* **104**, 062210 (2021).
- [75] C. Purkait and A. Biswas, Measurement-based quantum otto engine with a two-spin system coupled by anisotropic interaction: Enhanced efficiency at finite times, *Phys. Rev. E* **107**, 054110 (2023).
- [76] C. Purkait, S. Dasgupta, and A. Biswas, Quasi-probability distribution of work in a measurement-based quantum otto engine, *Physica A: Statistical Mechanics and its Applications* **673**, 130650 (2025).
- [77] N. Behzadi, Quantum engine based on general measurements, *Journal of Physics A: Mathematical and Theoretical* **54**, 015304 (2020).
- [78] S. R. Rathnakaran and A. Biswas, Ancilla measurement-based quantum otto engine using double-pair spin architecture, *Phys. Rev. E* **111**, 064116 (2025).
- [79] V. F. Lisboa, P. R. Dieguez, K. Simonov, and R. M. Serra, Correlations in a quantum switch-based heat engine with measurements: a proof-of-principle demonstration, *Quantum Science and Technology* **11**, 015058 (2026).
- [80] F. Mayo and A. J. Roncaglia, Enhancing the efficiency of quantum measurement-based engines with entangling measurements, *Phys. Rev. E* **113**, 014118 (2026).
- [81] K. Koshihara and K. Yuasa, No-go theorem for quantum heat engines powered purely by quantum measurements in the steady regime, *arXiv:2604.22376* (2026).
- [82] K. Maruyama, F. Nori, and V. Vedral, Colloquium: The physics of maxwell's demon and information, *Reviews of Modern Physics* **81**, 1–23 (2009).
- [83] D. Reeb and M. M. Wolf, An improved landauer principle with finite-size corrections, *New Journal of Physics* **16**, 103011 (2014).
- [84] P. Chattopadhyay, A. Misra, T. Pandit, and G. Paul, Landauer principle and thermodynamics of computation, *Reports on Progress in Physics* **88**, 086001 (2025).